



A validation of dynamic hygrothermal model with coupled heat and moisture transfer in porous building materials and envelopes

Wenqiang Dong ^{a,b}, Youming Chen ^{a,b,*}, Yang Bao ^{a,b}, Aimin Fang ^{a,b}

^a College of Civil Engineering, Hunan University, Changsha, Hunan, 410082, China

^b Key Laboratory of Building Safety and Energy Efficiency of the Ministry of Education Hunan University, Changsha, Hunan, 410082, China



ARTICLE INFO

Keywords:

Porous building materials and envelopes
Hygrothermal model
Theoretical validation
Inter-model validation
Experimental validation
Simulation

ABSTRACT

For predicting and evaluating the hygrothermal performance of buildings, predicting the risk of mould growth and improving the durability of the structure, an accurate dynamic hygrothermal model for coupled heat and moisture transfer in porous building materials and envelopes is necessary. The dynamic hygrothermal models need to be fully validated. However, literature review revealed that these models have not been fully validated. This study fully validates the Künzel model and the Liu model which are popular but not comprehensively validated. The results of both the models simulated by Fortran code and COMSOL Multiphysics are compared with analytical solutions, other model simulated solutions, and the data from two published experimental datasets. The simulated results of both models are in good agreement with the results in the existing published literature. All errors between the simulated and experimental results are within acceptable levels within the hygroscopic range. Near over-hygroscopic region (relative humidity is less than but close to 95%), the Liu model is more accurate than the Künzel model. The investigations in this study demonstrate that the two models are accurate and applicable for hygrothermal simulations within the hygroscopic range, the Künzel model is not applicable near over-hygroscopic region. It also boosts confidence for the application of two dynamic models for coupled heat and moisture transfer in building hygrothermal simulations.

1. Introduction

The heat and moisture transfers in porous building materials and envelopes often occur simultaneously in a highly coupled and nonlinear process. It is challenging to establish accurate models for the coupled heat and moisture transfer in porous building materials and envelopes. The moisture migration has a significant impact on the energy performance of envelopes, the quality of indoor environments and the durability of structures. After several decades' research and development, hygrothermal models were implemented in many fields of building engineering such as building energy consumption study [1–7], mould risk predictions [8–11] and the durability survey of structures [11–15].

(1) Building energy consumption

Due to the high thermal conductivity of water, the thermal conductivity of the material increases significantly with moisture transfer, which affects the sensible heat transfer through the building wall. For example, the thermal conductivity increases more than twice with the

moisture content increasing to full saturation for lime silica brick [16]. F. Kong's [4] investigation showed that the moisture migration and accumulation in the envelopes in the severe cold area increased the thermal conductivity of the wall, and increased the heat load by 5.2–13.6%. Santos's [5] investigation showed that disregarding the moisture transfer may cause great discrepancy on the prediction of hygrothermal performance in building engineering. Liu & Wang's [6] investigation showed that the energy consumption of an air conditioning system for the case of pine board house can be decreased about 40% and the air-conditioning operation time can be decreased due to the moisture effect. Liu's [7] investigation showed that ignoring the moisture effect may overestimate the peak cooling and heating loads by up to 2.1–3.9% and 4.2–10.1% and underestimate the yearly integrated loads by up to 4.4–6.8%.

(2) Mould risk predictions

Studies have pointed that the concentration of microorganisms rose rapidly from 400 ug/m³ to 2080 ug/m³ in buildings, when the moisture

* Corresponding author. College of Civil Engineering, Hunan University, Changsha, Hunan, 410082, China.

E-mail address: ymchen@hnu.edu.cn (Y. Chen).

content was increased from 7 g/kg to 15 g/kg [17]. In addition, moisture accumulation in the building materials can cause corrosion and chemical changes in the organic material and is conducive to the growth of mould. Mould is one of the main sources of indoor air pollution, and extremely harmful to human health. Studies have shown that when the relative humidity in the material reaches 80% and above, the mould will grow rapidly at a temperature suitable for human habitation [18]. How to properly control the humidity in the envelopes becomes the key to controlling mould. The VTT model [8,9] is a mould growth risk prediction model in which the mould index (M) is used to describe the mould growth. The mould growth is assessed by the mould index varying from 0 to 6. Jensen et al. [10] and Otiv [11] used the hydrothermal simulation tool Delphin to study mould risk predictions of internally insulated solid masonry walls. Their investigation showed that a reduction of the indoor relative humidity to 40% for the walls with hydrophobization decreased the mould growth risk at the interface during the whole year.

(3) Durability of structures

The differences in moisture content and temperature in porous building walls cause the moisture to migrate within the wall. When the wall temperature reduces to the dew point temperature of the air in the pores, the water vapor condenses in the wall, which results in a large accumulation of moisture. Christian's [19] investigation showed that a wood house released a total of 200 l water, in which had 19% moisture content; and per cubic meter of concrete released 90 l of moisture. Moisture accumulation will cause leakage, erosion, mould growth and other phenomena on the surface of the wall. Furthermore, moisture can also reduce the mechanical strength of building materials, which will cause the destructive deformation or even cracking of the envelopes and affect the safety and durability of the building structure. The durability of structures depends first on their capacity to keep dry and secondly on their drying capacity [12]. A method was developed by Altirkistani et al. [13] to quantify the drying capacity and the percentage of moisture movement out of the different building envelope systems. Otiv's [11] investigation showed that about 40% degradation would occur at the center of the brick layer and between the insulation and brick layer each year when the hydrophobic impregnation was not applied. Viitanen et al. [14] presented wood decay models and it was suitable for post-processing humidity and temperature data from numerical simulations of heat and humid conditions in building envelopes. Nofal et al. [15] developed a wood damage model with fluctuating temperature and moisture loading conditions to assess the durability of building envelopes.

Therefore, in order to realize the application of hydrothermal models in the above three aspects, it is of necessity to study and develop accurate models for the coupled heat and moisture transfer. A comprehensively validated and widely applicable dynamic model for the coupled heat and moisture transfer is the foundation for studying the hydrothermal performance of porous building materials and envelopes.

Research on simultaneous heat and moisture transfer in porous building materials and envelopes has been conducted for more than 70 years, and several theoretical models have been developed [20–23]. However, the study of simultaneous heat and moisture transfer is more difficult than the study of pure heat transfer because the moisture transfer mechanism is more complex and includes surface emission, diffusion and capillary conduction [24]. Moreover, the driving potentials and assumptions of each theoretical model are different, and there is no unified theoretical model to describe the heat transfer and moisture migration in building envelopes.

Berger and Pei [22] divided the total moisture transfer into two parts: one is the flow of liquid water under the capillary pressure gradient and the other is the vapor diffusion under the water vapor pressure gradient. However, since the physical parameters in the governing equation are difficult to obtain, and the solution is very

complicated, it is difficult to verify the model. Mendes et al. [25] proposed a heat and moisture transfer model for a multilayer wall driven by the temperature and moisture volume gradients and studied several simplified models of heat and moisture transfer for various common building materials under different boundary conditions. However, the author did not validate the model [26].

In summary, validation of hydrothermal models has become one of the focuses of research on coupled heat and moisture transfer in building envelopes. Do the existing assumptions and models for building hydrothermal simulations work well? It is necessary to implement a thorough investigation on the model validation for hydrothermal simulations. The main goals of this study are to review the model validation work in the field of coupled heat and moisture transfer in building envelopes, to summarize the validation methods of the dynamic coupled heat and moisture transfer models, and to validate the Künzel model and the Liu model in the existing literature through a comprehensive comparison of their simulation results with the simulation and experimental results published in the literature.

2. Literature review

2.1. Models

The main difference among various hydrothermal models for porous building materials and envelopes is the driving potential of the moisture migration. The moisture driving potentials used in the hydrothermal models in existing literature include partial water vapor pressure, moisture content, capillary pressure, relative humidity, and air moisture content.

Hagentoft [27] established a coupled model of the heat, air and moisture of the envelope structure that used temperature, partial water vapor pressure and air pressures as driving potentials. Five benchmark cases [28] can validate the built hydrothermal models.

Kong [29] simulated the heat and moisture coupling of the drying process of the single-layer slag concrete block wall in a severely cold area. The moisture content gradient was used as the mass transfer driving potential. An experiment under real external climatic conditions was implemented, and the simulation results were compared with the experimental results to validate the correctness of the model.

A numerical model was developed by Pedersen [30] for the combined heat and moisture transport in composite building constructions based on the moisture potential of capillary suction pressure. Qinru Li [31] developed an advanced numerical tool that were multi-dimensional and dynamic couplings of heat and moisture transfer driven by capillary suction pressure and temperature. This tool used COMSOL Multiphysics [32] to solve the governing equations. This numerical tool was well suited to the benchmark cases [28], and the predictions showed good agreement with the data of full-scale wall experiments.

Künzel [33] used the relative humidity instead of the moisture content of the material as the moisture driving potential to establish the coupled model and used three experimental test examples exposed to real weather conditions to validate the established hydrothermal model. The measured results agreed well with the calculation results. Liu and Chen [34] developed a coupled heat and moisture transfer model to calculate the conducted heat load through the building envelope. It was solved by using COMSOL Multiphysics and validated by comparing the results with the benchmark cases of EN 15026 [35,36] and the HAMSTAD project [28].

To avoid the problem of discontinuity in moisture content at the interface of multilayer walls, Budaiwi et al. [37] and Guo [38] used the temperature and air moisture content as the driving potentials to establish coupled heat and moisture transfer models for multilayer walls. Budaiwi's model was validated by comparing the program predictions with the basic theoretical solutions and the results of representative experimental tests. Guo's model prediction results were

compared with the experimental test data, and they were in good agreement.

Vapor density [39,40] or logarithmic capillary pressure [41] was also used as the driving potential for moisture transfer in some research studies.

2.2. Validation

The purpose of model validation is to: i) validate the correctness of the model, including the governing equations and boundary conditions; and ii) validate the accuracy of the numerical solution. Künzel and Karagiozis [42] divided the rigorous validation of a hygrothermal simulation model into three steps. The first step is to validate the correct implementation of the physical foundation by comparing it with the analytical solution. The second step is to compare the calculations and laboratory tests with well-defined material data and boundary conditions. The third step is to simulate the dynamic hygrothermal performance of a building envelope exposed to a real external climate. If the simulation and experimental results are consistent, the model validation of the building envelope component is successful.

Obviously, the validation are not sufficient for the above mentioned hygrothermal models of couple heat and moisture transfer in porous building materials and envelopes. Some models have no experimental validation or only relatively simple experimental validation. Therefore, a comprehensive validation is very necessary to further boost confidence for the application of the dynamic models for coupled heat and moisture transfer in building hygrothermal performance simulation such as building energy consumption study, mould risk predictions and the durability survey of structures.

In summary, there are three methods commonly used to validate models: theoretical validation (comparison with analytical solutions), inter-model validation (comparison with the simulated results of other models), and experimental validation (comparison with experimental test data). The model validation methods are summarized in Table 1.

(1) Theoretical validation

Theoretical validation is an accurate and effective validation method, but it can only be applied to cases of simple analytical solutions. For multilayer enclosures, the governing equations are highly nonlinear and coupled to each other, which makes it impossible to accurately obtain the analytical solution.

(2) Inter-model validation

This method can be divided into two categories: comparison with the numerical results of previous research literature and comparison with the simulated results of hygrothermal simulation software, such as WUFI [43] and Delphin [44].

Theoretical validation and inter-model validation are implemented by numerical methods. The common numerical methods are divided into three types: i) the PDE module of the finite element software COMSOL Multiphysics [45]; ii) hygrothermal simulation software, such

as WUFI [46–48], Delphin [49,50], etc; iii) self-programming calculation.

(3) Experimental validation

Experiments are the most effective and important method to validate coupled heat and moisture transfer models. The accuracy of model prediction is assessed by comparing the numerical results of the models with the experimental data. Researchers [51–53] have conducted several experimental studies on model validation. Busser [54] reviewed the recent experimental studies to validate the hygrothermal models for building materials and envelopes. He divided the experimental facilities into two scales: material and wall. The material scale includes two types, climate chamber and air tunnel. These facilities differed only in controlling convective boundary conditions, and both can be used to study the hygrothermal behaviours of a single material exposed to controlled conditions. The wall scale can be divided into exposure to controlled conditions in the climate chamber or natural outdoor conditions on one side.

The experiments to validate models can be divided into two types: under controlled conditions (including one-sided and doubled-sided response) and exposure to real external climatic conditions (including single-layer and multilayer walls).

3. Comprehensive validation for two models

To provide solid and credible coupled heat and moisture transfer models for researchers and users to accurately predict and evaluate the hygrothermal behaviour and performance of porous building envelopes and entire buildings, a comprehensive validation was performed to validate the Künzel model [33] and the Liu model [34], which are the commonly used hygrothermal models.

These two models were chosen because of the following: i) the moisture driving potential is relative humidity, which is easy to measure; ii) the moisture driving potential is continuous at the interface of a multilayer wall, making simulation calculations easier to implement; and iii) the two models are popular but not fully validated.

The comprehensive validation in this section includes theoretical, inter-model and experimental validation. The solutions for the two models were numerically calculated by Fortran code and COMSOL Multiphysics for all cases of validation. The details of the two models are described below.

3.1. Mathematical model

The process of coupled heat and moisture transfer through a porous multilayer wall is illustrated in Fig. 1. The assumptions for the two models are that no air transfer occurs; the effect of gravity is negligible; the temperatures remain well below the boiling temperature of water; the effects of icing and melting processes are neglected; only gas and liquid are in the pores; wet air is treated as an ideal gas; and there is only one-dimensional heat and moisture transfer. In Fig. 1, the symbol Q is the heat flow and the symbol S is the moisture flow from outside to inside.

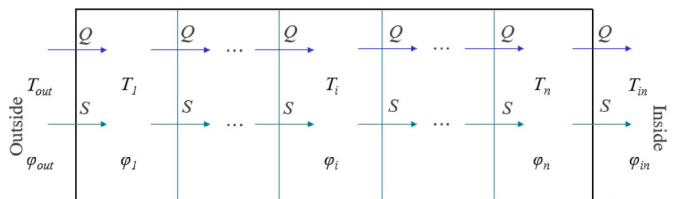


Fig. 1. Schematic for coupled heat and moisture transfer through a porous multilayer wall.

Table 1
Summary of reported studies for model validation methods.

Validation methods	References	
Theoretical validation	[28,31,34,36,37,41]	
Inter-model validation	numerical simulated software	[28,31,34,41] [46–50]
Experimental validation	controlled conditions	one-sided [30,56] double-sided [31,37,39,40,50]
	real conditions	single layer [29] multilayer [33,38,41]

3.1.1. Künzel model

The Künzel model is established in the literature [33] and uses relative humidity ϕ as the moisture driving potential. In this model, the moisture transfer in the porous media is treated as a pure diffusion process, which is described by Fick's law.

The heat and moisture governing equations are given by Eqs. (1) and (2).

$$\frac{\partial H}{\partial T} \frac{\partial T}{\partial t} = \frac{\partial}{\partial x} \left(\lambda \frac{\partial T}{\partial x} \right) + h_{lv} \frac{\partial}{\partial x} \left(\frac{\delta_a}{\mu} \frac{\partial (\phi P_{sat})}{\partial x} \right) \quad (1)$$

$$\frac{\partial w}{\partial t} \frac{\partial \phi}{\partial t} = \frac{\partial}{\partial x} \left(D_w \frac{\partial w}{\partial \phi} \frac{\partial \phi}{\partial x} \right) + \frac{\partial}{\partial x} \left(\frac{\delta_a}{\mu} \frac{\partial (\phi P_{sat})}{\partial x} \right) \quad (2)$$

where $\delta_a = 2 \times 10^{-7} \times (T + 273.15)^{0.81} / P_{ambient}$, $\partial H / \partial T = (\rho_m c_{p,m} + c_{p,l} w)$, δ_a (kg/(m·s·Pa)) is the water vapor permeability of stagnant air, μ (–) is the water vapor diffusion resistance factor, D_w (m²/s) is the capillary transport coefficient (moisture diffusivity), H (J/m³) is the total enthalpy, $P_{ambient}$ (Pa) is the ambient atmospheric pressure, ϕ (%) is the relative humidity, T (K) is the temperature, t (s) is the time coordinate, P_{sat} (Pa) is the saturated water vapor pressure, which is a function of temperature T (K), w (kg/m³) is the moisture content, ρ_m (kg/m³) is the density of the dry material, $c_{p,m}$ (J/(kg·K)) is the specific capacity of the dry material, h_{lv} (J/kg) is the latent heat of evaporation, λ (W/(m·K)) is the thermal conductivity, and $c_{p,l}$ (J/(kg·K)) is the specific heat of liquid water.

3.1.2. Liu model

The Liu model can be found in the literature [34]. In this model, the temperature and relative humidity are used as the driving potentials to avoid the problem of moisture driving a potential discontinuity at the interface between two different porous media. In this model, vapor diffusion is described by Fick's law, and liquid water transfer is described by Darcy's law.

The heat and moisture governing equations are given by Eqs. (3) and (4).

$$(\rho_m c_{p,m} + c_{p,l} w) \frac{\partial T}{\partial t} = \nabla \left(\left(\lambda + h_{lv} \delta_p \phi \frac{dP_{sat}}{dT} \right) \nabla T + h_{lv} \delta_p P_{sat} \nabla \phi \right) \quad (3)$$

$$\xi \frac{\partial \phi}{\partial t} = \nabla \left(\left(\delta_p \phi \frac{dP_{sat}}{dT} + K_l \rho_l R_D \ln(\phi) \right) \nabla T + \left(\delta_p P_{sat} + K_l \rho_l R_D \frac{T}{\phi} \right) \nabla \phi \right) \quad (4)$$

where δ_p (kg/(m·s·Pa)) is the water vapor permeability, K_l (s) is the liquid water permeability, ρ_l (kg/m³) is the density of liquid water, R_D (J/(kg·K)) is the gas constant of water vapor, and $\xi = \partial w / \partial \phi$ is the sorption capacity (the slope of the sorption-moisture retention curve).

3.1.3. Boundary conditions

Both models use the same boundary conditions. The solar radiation is considered the external heat boundary condition.

The outer and inner surface boundary conditions are given by Eqs. (5)–(8).

$$g_{n,e} = \beta_{p,e} (\phi_e p_{sat,e} - \phi_{surf,e} p_{sat,surf,e}) \quad (5)$$

$$q_{n,e} = h_e (T_e - T_{surf,e}) + h_{lv} \cdot g_{n,e} + \alpha \cdot q_{solar} \quad (6)$$

$$g_{n,i} = \beta_{p,i} (\phi_i p_{sat,i} - \phi_{surf,i} p_{sat,surf,i}) \quad (7)$$

$$q_{n,i} = h_i (T_i - T_{surf,i}) + h_{lv} g_{n,i} \quad (8)$$

where ϕ_e is the relative humidity of outdoor air, T_e (K) is the temperature of outdoor air, ϕ_i is the relative humidity of the indoor air, T_i (K) is the temperature of indoor air, g_n (kg/(m²·s)) is the moisture flow through the wall surface, q_n (W/m²) is the heat flow across the surface,

β_p (kg/(m²·s·Pa)) is the vapor transfer coefficient at the surface, ϕ_{surf} is the relative humidity at the surface, p_{sat} (Pa) is the saturation water vapor pressure of air, $p_{sat,surf}$ (Pa) is the saturation water vapor pressure on the surface, h (W/(m·K)) is the heat transfer coefficient at the surface, T_{surf} (K) is the temperature at the surface, α is the solar absorptivity of the exterior surface of the exterior wall, q_{solar} (W/m²) is the solar radiation, and the subscript e/i refers to the exterior/interior surface of the wall.

3.1.4. Model difference

Vapor diffusion and liquid water transfer are both described by Fick's law for Künzel model [24,33]. But in fact, the capillary transfer of liquid water is a kind of "flow" rather than "diffusion". Moreover, the two "diffusion" of vapor diffusion and liquid water transfer in the building material are opposite, ignoring the interaction of the two "diffusion", and treating the two as two independent processes [38].

For Liu model, vapor diffusion is described by Fick's law, and liquid water transfer is described by Darcy's law. And moisture diffusivity D_w contains two parts: liquid water transfer and water vapor diffusion, that is to say, there is a functional relationship between D_w , K_l and δ_p , which is $K_l = (D_w \xi - \delta_p P_s) \phi / (R_D T \rho_l)$ [27].

3.2. Solving methods

In all verification cases, the numerical solutions of the two models are calculated by a Fortran code and COMSOL Multiphysics. The Fortran code is developed with the Crank-Nicholson scheme [55], which is used to discretize the governing equations of the hygrothermal models. A remarkable feature of this scheme is that many coefficients are unknown. Therefore, it is a set of typical nonlinear equations. The Newton iteration method transforms nonlinear equations into linear equations, and then the Gauss elimination method is used to solve these linear equations. In the Fortran code, the time step varies from 60–3600 s, and the space step varies from 2–10 mm. The convergence criterion is 10⁻⁴, and the maximum iteration number is set to 30.

3.3. Model validation

A comprehensive validation for the Künzel model and the Liu model was implemented in this section. The three methods described in Section 2.2 were used to verify these two models. Both the models were simulated using the Fortran code and COMSOL Multiphysics. The simulation results were compared with analytical solutions, simulation results of other models and experimental data to verify the accuracy of the two models. In addition, comparisons between the simulation results of the two models were made. In the comparisons, "Künzel + Fortran" refers to the simulation results of the Künzel model with Fortran code; "Künzel + Comsol" refers to the simulation results of the Künzel model with COMSOL Multiphysics; "Liu + Fortran" refers to the simulation results of the Liu model with Fortran code; and "Liu + Comsol" refers to the simulation results of the Liu model with COMSOL Multiphysics.

The maximum relative error was used to assess the consistency of the simulation results with the analytical solution and the simulation solutions of other models. The mean error (ME) and the root mean square error (RMSE) were simultaneously used to assess the consistency of the simulation results with the experimental results.

$$ME = \frac{\sum |y_{meas} - y_{sim}|}{n} \quad (9)$$

$$RMSE = \sqrt{\frac{\sum (y_{meas} - y_{sim})^2}{n}} \quad (10)$$

where y_{meas} is the experimental measured values, y_{sim} is the model simulation results, and n is number of values.

3.3.1. Theoretical validation

HAMSTAD Benchmark case #2 [28] was implemented as an example for theoretical validation. This benchmark describes the moisture redistribution in a homogeneous single layer wall under isothermal conditions. Since the temperature difference through the interior and exterior of the wall is eliminated, an analytical solution can be obtained. The thickness of the wall is 200 mm. The layer is initially in moisture equilibrium with the ambient air, which has constant relative humidity. Moisture movement is caused by a sudden change in the relative humidity in the surroundings. The exterior air temperature and relative humidity conditions are 20 °C and 45%, respectively; the interior air temperature and relative humidity conditions are 20 °C and 65%, respectively. The initial wall temperature and relative humidity are 20 °C and 95%, respectively. The heat and mass transfer coefficients are 25 W/(m²·K) and 1.0×10^{-3} s/m, respectively. The material properties are presented in Table A.1. The simulation lasts 1000 h. The required outputs are the moisture content distributions across the wall at 100, 300 and 1000 h.

The simulation results of the two models with Fortran code and COMSOL Multiphysics were compared with the analytical solutions. The comparison results are shown in Fig. 2. The maximum relative errors of the Künzel model with Fortran code are 2.56% at 100 h, 1.06% at 300 h and 0.45% at 1000 h. Correspondingly, the maximum relative errors of the Liu model with Fortran code are 2.62% at 100 h, 1.07% at 300 h and 0.45% at 1000 h. In addition, the calculation results of the two models agree well with the analytical solutions, and the calculation results with Fortran code and COMSOL Multiphysics are very consistent.

3.3.2. Inter-model validation

HAMSTAD Benchmark case #5 [28] was implemented as an example for inter-model validation. In this benchmark case, the moisture redistribution in a three-layer composite wall is analysed. The three layers of the wall are: 365 mm of brick at the exterior as a load bearing layer, followed by 15 mm of mortar, and finally, a 40 mm insulation layer in the interior. The exterior air temperature and relative humidity conditions are 0 °C and 80%, respectively; the interior air temperature and relative humidity conditions are 20 °C and 60%, respectively. The heat transfer coefficients of the interior and exterior surfaces are 8 W/(m²·K) and 25 W/(m²·K), respectively. The mass transfer coefficients of the interior and exterior surfaces are 5.8823×10^{-8} s/m and 1.8382×10^{-7} s/m, respectively. The initial temperature and relative humidity for the various layers of the wall are 25 °C and 60%, respectively. The material properties of each layer are given in Table A.2 and A.3. The relative

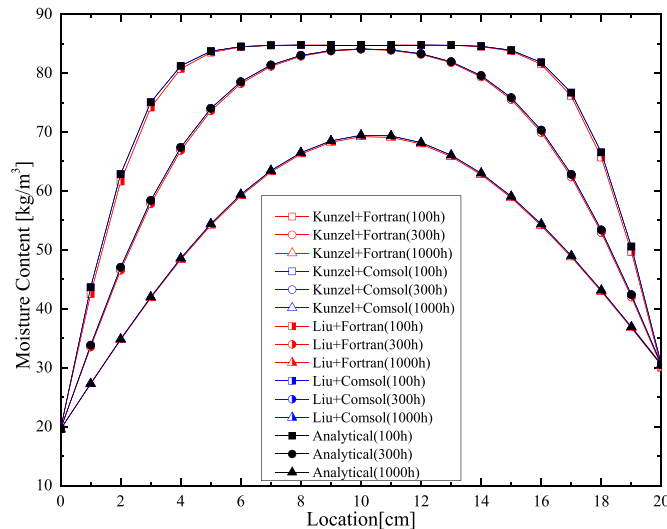


Fig. 2. Moisture content profiles of the homogeneous single wall at 100, 300 and 1000 h.

humidity and moisture content profiles at the end of 60 days are shown in Fig. 3, in which “TUD” refers to the simulated results provided by the Technical University of Dresden [28].

The simulation results of the Liu model with Fortran code and COMSOL Multiphysics are compared with the TUD results. The comparison results are shown in Fig. 3. The maximum relative errors of the Künzel model for relative humidity with Fortran code and COMSOL Multiphysics are 11.7% and 10.1%, respectively. The maximum relative errors of the Liu model for relative humidity with Fortran code and COMSOL Multiphysics are 1.58% and 0.54%, respectively. Also, the simulation results of the Liu model with Fortran code and COMSOL Multiphysics agree well with the TUD results. However, near over-hygroscopic region (relative humidity is close to 95%), the simulation results of the Künzel model are significantly different.

3.3.3. Experimental validation: one-side controlled conditions

3.3.3.1. Experiment. A published experiment dataset [56–58] under one-sided controlled conditions was used to validate the Künzel model and the Liu model. Scots pine was chosen as the test material, and the relative humidity and temperature at different depths (1, 4 and 7 mm from the front) of the sample were monitored. The material properties used in the simulation [27,58–61] are presented in Table A.4. The relative humidity in the ambient climate chamber varied between 35 and 75% in 10-day long step changes. The measured data of the relative humidity and temperature at the different depths and boundary conditions were recorded for 100 days with a sampling interval of 30 min. The step change from the 40th to 60th days covered an interval of 20 days. The other step changes all covered an interval of 10 days. The surface heat and mass transfer coefficients are 25 W/(m²·K) and 1.925×10^{-7} s/m, respectively.

3.3.3.2. Validation. The relative humidity and temperature at the depth of 4 mm were calculated by the Künzel model and the Liu model with Fortran code and COMSOL Multiphysics. The simulation results of the Künzel model and the Liu model with the Fortran code and COMSOL Multiphysics were compared with the experimental data. The comparison between the simulated and measured relative humidity/temperature at the depth of 4 mm is illustrated in Fig. 4.

As indicated in Fig. 4, the simulated results of the two models agree well with the measured data. During desorption, the simulated relative humidity of the two models are both underestimated, and during adsorption, the simulation results of the relative humidity are both overestimated compared with the measured data.

The MEs and RMSEs between the simulated and measured relative humidity/temperature at the depth of 4 mm are given in Table 2. Kunzel + Fortran and Kunzel + Comsol have the maximum MEs of relative humidity and temperature which are 4.61% and 0.11 °C, respectively. Kunzel + Fortran and Kunzel + Liu + Fortran have the maximum RMSEs of relative humidity and temperature which are 5.37% and 0.44 °C, respectively. The simulated results of the two models are in a good agreement with the measured data, and the simulated results of the two methods are very consistent. Additionally, the simulated values of the Liu model are closer to the measured values than are the simulated values of the Künzel model during desorption.

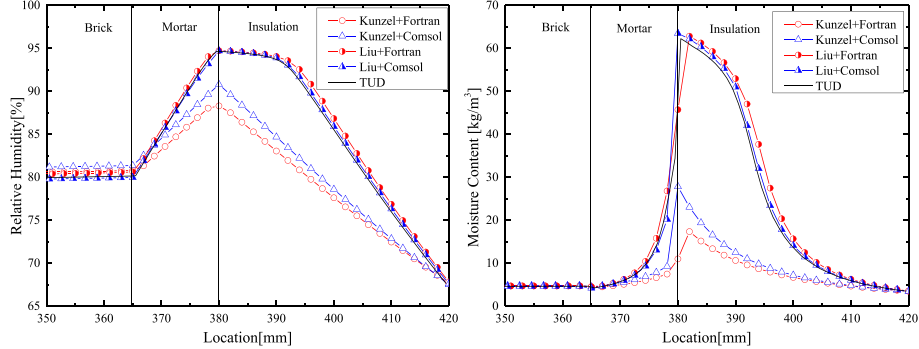
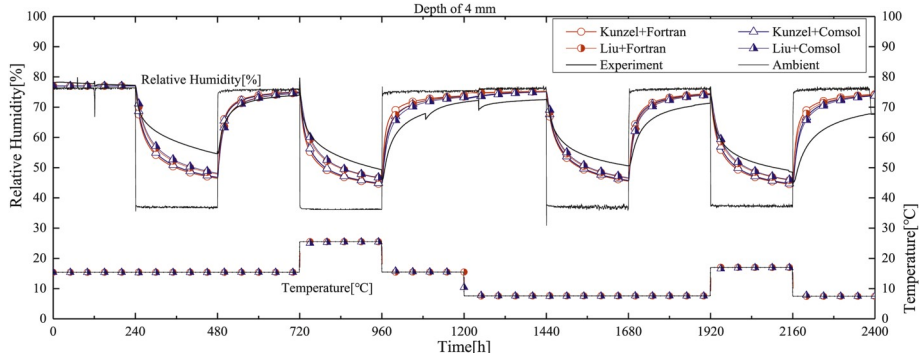
3.3.4. Experimental validation: double-side controlled conditions

3.3.4.1. Experiment. Another published experiment dataset [62] under double-sided controlled conditions was used to further validate the accuracy of the two models. The experiment was implemented in a double climatic chamber. The relative humidity and temperature in the two chambers and inside the materials were measured. The schematic of the climatic chamber, configuration of each tested wall and locations of the sensors in each wall are shown in Figs. 5 and 6. The climate conditions

Table 2

ME and RMSE between measured and simulated results at the depth of 4 mm.

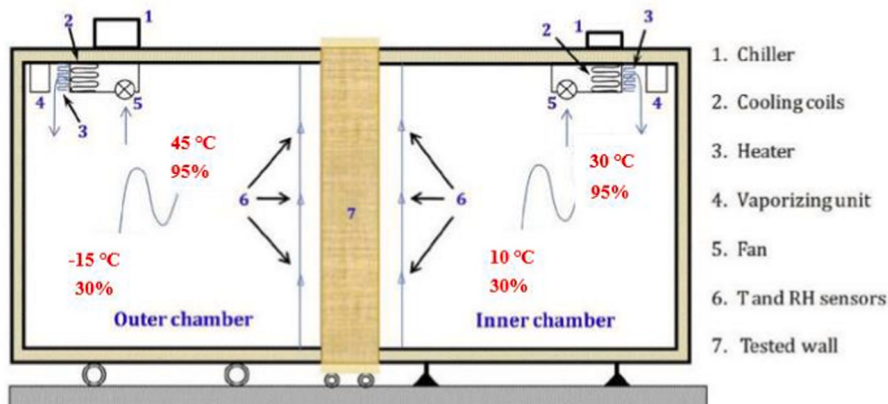
	ME				RMSE			
	Kunzel + Fortran	Kunzel + Comsol	Liu + Fortran	Liu + Comsol	Kunzel + Fortran	Kunzel + Comsol	Liu + Fortran	Liu + Comsol
Relative Humidity [%]	4.61	4.06	3.56	3.17	5.37	4.74	4.33	3.82
Temperature [°C]	0.044	0.11	0.038	0.11	0.44	0.28	0.44	0.28

**Fig. 3.** Relative humidity (left) and moisture content (right) profiles at the end of 60 days.**Fig. 4.** Comparison between the simulated and measured results at the depth of 4 mm.

were measured at each wall. The climate conditions of Wall #4 in the two chambers are shown in Fig. B.1, in which “RHout” refers to the external relative humidity, “RHin” refers to the indoor relative humidity, “Tout” refers to the external temperature, and “Tin” refers to the indoor temperature. The simulation results for each wall have a time step of 1 h, because both the climate information and the measurement results were provided as hourly data. More information about the

chamber, climatic conditions, instrumentations and materials is described in the literature [62].

The material properties of the four walls in the simulation are obtained from the Delphin material database [44], and the data are measured by Rafidirason et al. [62] and Vololonirina et al. [63], as partially listed in Table A.5. The initial conditions are determined by the first values of the experimental measurements corresponding to the

**Fig. 5.** Schematic of the climate chamber [62].

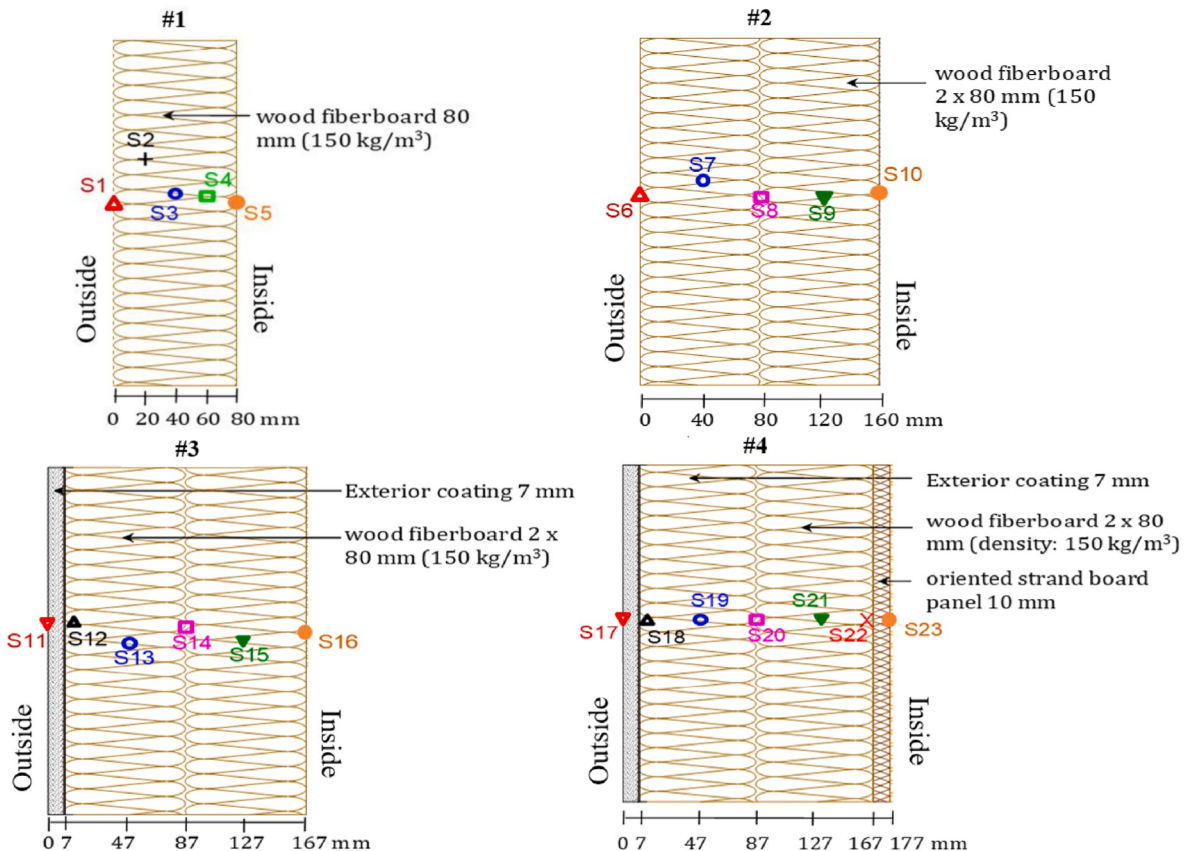


Fig. 6. Schematic of the wall configurations and the sensor locations in the tested walls [62].

centre of the tested wall. The surface heat transfer and mass transfer coefficients [64] at the two sides of the walls are listed in Table A.6.

3.3.4.2. Validation. The relative humidity and temperature were simulated by using the Fortran code and COMSOL Multiphysics on the Künzel model and Liu model. The measured data shown in Fig. B.1 were used as boundary conditions of the simulation. The simulation results were compared with the experimental data to validate the accuracy of the two models. The simulation results for each wall are separately discussed as follows. The quality of the hygrothermal models was evaluated using the ME and RMSE between the simulation and experiment results.

(1) Wall #1

The configuration of Wall #1, which consists of 80 mm of wood fibreboard, is shown in Fig. 6. Fig. B.2–B.6 show the comparisons between the simulation and measured results of Wall #1.

In Fig. B.2–B.6, the simulated values of the relative humidity are almost always higher than the measured values. Fig. B.2–B.6 show the results at different depths, and the results of the Künzel model and the Liu model by Fortran code and COMSOL Multiphysics exhibit the same

trend but differ in the measurements. In addition, the simulated values by the Künzel model are closer to the measured values than are the simulated values by the Liu model at the depths of 20 mm, 40 mm, and 60 mm.

Tables 3 and 4 show the MEs and RMSEs of the simulated relative humidity and temperature in Wall #1, respectively. The MEs and RMSEs of the relative humidity and temperature simulated by the Künzel model and the Liu model are very close at each measurement location in the wall. The ME of the relative humidity at all measurement locations is within the range of 1.85–3.85%. The RMSE of the relative humidity at all measurement locations is within the range of 2.02–4.44%. The ME of the temperature at all measurement locations is within the range of 0.18–0.86 °C. Finally, the RMSE of the temperature at all measurement locations is within the range of 0.24–1.16 °C. The computation programs (Fortran code and COMSOL Multiphysics) have very little effect on the simulation results. For Wall #1, the two models have a good agreement with the experimental results, and the ME and RMSE of the relative humidity and temperature are within the acceptable levels.

(2) Wall #2

Wall #2 has a thickness of 160 mm and consists of two layers of wood

Table 3

ME and RMSE between the simulated and measured relative humidity at each measurement location in Wall #1.

Sensor locations	ME [%]				RMSE [%]			
	Künzel + Fortran	Künzel + Comsol	Liu + Fortran	Liu + Comsol	Künzel + Fortran	Künzel + Comsol	Liu + Fortran	Liu + Comsol
External	3.56	3.84	3.85	3.83	4.09	4.43	4.44	4.42
20 mm	2.63	3.22	3.24	3.23	2.89	3.58	3.59	3.61
40 mm	2.35	2.96	2.96	2.97	2.56	3.44	3.43	3.46
60 mm	2.61	2.80	2.78	2.79	2.83	3.28	3.26	3.28
Internal	2.13	1.85	1.87	1.85	2.25	2.02	2.13	2.02

Table 4

ME and RMSE between the simulated and measured temperature at each measurement location in Wall #1.

Sensor locations	ME [°C]				RMSE [°C]			
	Kunzel + Fortran	Kunzel + Comsol	Liu + Fortran	Liu + Comsol	Kunzel + Fortran	Kunzel + Comsol	Liu + Fortran	Liu + Comsol
External	0.84	0.86	0.86	0.86	1.16	1.16	1.16	1.16
20 mm	0.47	0.50	0.50	0.50	0.55	0.58	0.58	0.59
40 mm	0.18	0.20	0.20	0.24	0.24	0.27	0.27	0.34
60 mm	0.35	0.38	0.38	0.38	0.39	0.42	0.43	0.44
Internal	0.40	0.41	0.41	0.41	0.48	0.49	0.49	0.48

fibreboard. [Fig. B.7–B.11](#) show the comparisons between the simulated and measured results of Wall #2. Because of missing and abnormal values in the measurements, the temperature peak in the interval between hours 1703 and 1755 was removed from the simulation.

[Figs. B.7–B.11](#) show the results at different depths, and the results of the Künzel model and the Liu model by Fortran code and COMSOL Multiphysics show the same trend but differ in the measurements. The simulated relative humidity values at depths of 40 mm and 80 mm exhibit a high compliance with the measured relative humidity values in [Figs. B.8–B.9](#). Furthermore, at a depth of 120 mm, the simulated values of the Künzel model are closer to the measured values than the simulated values of the Liu model.

[Tables 5 and 6](#) present the MEs and RMSEs of the simulated relative humidity and temperature in Wall #2, respectively. The MEs and RMSEs of the relative humidity and temperature simulated by the Künzel model and the Liu model are very small at each measurement location in the wall. The ME of the relative humidity at all measurement locations is within the range of 1.51–2.72%. The RMSE of the relative humidity at all measurement locations is within the range of 1.81–3.20%. The ME of the temperature at all measurement locations is within the range of 0.19–0.84 °C. Finally, the RMSE of the temperature at all measurement locations is within the range of 0.27–1.08 °C. The computation programs (Fortran code and COMSOL Multiphysics) have very little effect on the simulation results. The two models exhibit good consistency with the experimental results for Wall #2. In addition, the MEs and RMSEs of the relative humidity and temperature are found to be within the acceptable levels.

(3) Wall #3

W #3 consists of an exterior lime plaster coating of 7 mm at the external side and 160 mm of wood fibreboard on the internal side. [Figs. B.12–B.17](#) show the comparison of the simulation and measured results of Wall #3.

[Figs. B.12–B.17](#) illustrate the results at different depths. The results of the Künzel model and the Liu model by Fortran code and COMSOL Multiphysics exhibit the same trend but differ in their measurements. There are the large deviations of more than 10% relative humidity between the simulated and measured relative humidity from approximately 1600–2200 h in [Fig. B.13–B.15](#). Additionally, at a depth of 7 mm, the simulated values of the Liu model are closer to the measured values than the simulated values of the Künzel model.

[Tables 7 and 8](#) show the MEs and RMSEs of the simulated relative humidity and temperature in Wall #3, respectively. The MEs and RMSEs

of the relative humidity and temperature simulated by the Künzel model and the Liu model are very small at each measurement location in the wall. The ME of the relative humidity at all measurement locations is within the range of 1.15–5.96%. The RMSE of the relative humidity at all measurement locations is within the range of 0.97–4.65%. The ME of the temperature at all measurement locations is within the range of 0.23–0.59 °C. Finally, the RMSE of the temperature at all measurement locations is within the range of 0.30–0.92 °C. The computation programs (Fortran code and COMSOL Multiphysics) have some effect on the simulation results for relative humidity, especially at the depth of 7 mm. For Wall #3, the two models have a good agreement with the experimental results, and the ME and RMSE of the relative humidity and temperature are within the acceptable levels.

(4) Wall #4

Wall #4 is shown in [Fig. 6](#) and differs from Wall #3 in that an OSB-board is applied at the side of the internal chamber. [Fig. B.18–B.24](#) present the comparison of the simulation and measured results of Wall #4.

[Figs. B.18–B.24](#) display the results at different depths, and the results of the Künzel model and the Liu model by Fortran code and COMSOL Multiphysics show the same trend but differ in the measurements. [Fig. B.19](#) shows the results at the location of 7 mm in Wall #4 for the temperature simulation and the relative humidity. In the left graph of [Fig. B.19](#), the peak in the measurement values before 500 h does not appear in the simulation results because of abnormal measurement values. The simulation results for the relative humidity at the depth of 167 mm deviate largely from the measurements in [Fig. B.23](#). Furthermore, at the external surface, the values simulated by the Liu model are closer to the measured values than are the values simulated by the Künzel model. However, at the depth of 47 mm, the simulated values by the Künzel model are closer to the measured values than are the simulated values of the Liu model.

[Tables 9 and 10](#) show the MEs and RMSEs of the simulated relative humidity and temperature of Wall #4, respectively. The MEs and RMSEs of the relative humidity and temperature simulated by the Künzel model and the Liu model are very small at each measurement location except at the depth of 167 mm. The ME of the relative humidity at all measurement locations is within the range of 1.05–6.25%. The RMSE of the relative humidity at all measurement locations is within the range of 0.51–7.52%. The ME of temperature at all measurement locations is within the range of 0.27–0.63 °C. The RMSE of the temperature at all measurement locations is within the range of 0.32–0.78 °C. The

Table 5

ME and RMSE between the simulated and measured relative humidity at each measurement location in Wall #2.

Sensor locations	ME [%]				RMSE [%]			
	Kunzel + Fortran	Kunzel + Comsol	Liu + Fortran	Liu + Comsol	Kunzel + Fortran	Kunzel + Comsol	Liu + Fortran	Liu + Comsol
External	2.51	2.71	2.72	2.71	2.93	3.19	3.20	3.19
40 mm	1.92	2.50	2.51	2.50	2.20	3.07	3.08	3.07
80 mm	1.51	2.18	2.18	2.18	1.81	2.78	2.77	2.78
120 mm	1.59	2.24	2.23	2.24	1.82	2.67	2.66	2.67
Internal	2.32	2.30	2.35	2.30	2.69	2.62	2.71	2.62

Table 6

ME and RMSE between the simulated and measured temperature at each measurement location in Wall #2.

Sensor locations	ME [°C]				RMSE [°C]			
	Kunzel + Fortran	Kunzel + Comsol	Liu + Fortran	Liu + Comsol	Kunzel + Fortran	Kunzel + Comsol	Liu + Fortran	Liu + Comsol
External	0.83	0.84	0.84	0.84	1.08	1.08	1.08	1.08
40 mm	0.19	0.24	0.24	0.24	0.27	0.31	0.31	0.31
80 mm	0.24	0.29	0.29	0.29	0.30	0.37	0.37	0.37
120 mm	0.25	0.28	0.28	0.28	0.32	0.35	0.35	0.35
Internal	0.34	0.35	0.35	0.35	0.47	0.49	0.49	0.49

Table 7

ME and RMSE between the simulated and measured relative humidity at each measurement location in Wall #3.

Sensor locations	ME [%]				RMSE [%]			
	Kunzel + Fortran	Kunzel + Comsol	Liu + Fortran	Liu + Comsol	Kunzel + Fortran	Kunzel + Comsol	Liu + Fortran	Liu + Comsol
External	2.41	1.56	2.41	1.49	1.78	1.73	1.76	0.97
7 mm	5.92	3.16	5.96	4.03	4.65	2.42	4.64	2.90
47 mm	4.30	4.44	3.86	4.89	3.44	2.88	3.28	3.21
87 mm	3.65	4.04	3.25	4.32	2.57	2.33	2.53	2.48
127 mm	2.97	3.30	3.51	3.45	1.69	1.90	1.97	2.00
Internal	1.15	1.19	1.16	1.21	1.36	1.46	1.45	1.49

Table 8

ME and RMSE between the simulated and measured temperature at each measurement location in Wall #3.

Sensor locations	ME [°C]				RMSE [°C]			
	Kunzel + Fortran	Kunzel + Comsol	Liu + Fortran	Liu + Comsol	Kunzel + Fortran	Kunzel + Comsol	Liu + Fortran	Liu + Comsol
External	0.59	0.58	0.59	0.58	0.92	0.91	0.92	0.91
7 mm	0.38	0.34	0.37	0.34	0.49	0.44	0.47	0.44
47 mm	0.23	0.38	0.26	0.39	0.30	0.54	0.33	0.55
87 mm	0.28	0.37	0.31	0.37	0.37	0.50	0.39	0.50
127 mm	0.23	0.30	0.24	0.30	0.30	0.40	0.32	0.40
Internal	0.28	0.30	0.35	0.30	0.39	0.41	0.45	0.41

Table 9

ME and RMSE between the simulated and measured relative humidity at different sensor locations in Wall #4.

Sensor locations	ME [%]				RMSE [%]			
	Kunzel + Fortran	Kunzel + Comsol	Liu + Fortran	Liu + Comsol	Kunzel + Fortran	Kunzel + Comsol	Liu + Fortran	Liu + Comsol
External	2.30	1.05	2.30	0.92	1.51	0.65	1.51	0.58
7 mm	2.81	4.00	2.81	4.44	2.05	2.18	2.05	2.73
47 mm	2.58	4.06	2.58	4.28	1.67	2.59	1.67	2.90
87 mm	3.08	3.63	3.20	3.86	2.04	2.07	2.37	2.07
127 mm	4.31	2.63	4.69	2.82	4.98	3.17	5.41	3.36
167 mm	5.97	2.80	6.25	2.80	7.17	3.37	7.52	3.33
Internal	2.16	1.30	2.04	1.51	0.84	0.51	0.85	0.56

Table 10

ME and RMSE between the simulated and measured temperature at different sensor locations in Wall #4.

Sensor locations	ME [°C]				RMSE [°C]			
	Kunzel + Fortran	Kunzel + Comsol	Liu + Fortran	Liu + Comsol	Kunzel + Fortran	Kunzel + Comsol	Liu + Fortran	Liu + Comsol
External	0.54	0.53	0.54	0.53	0.47	0.46	0.47	0.46
7 mm	0.51	0.49	0.50	0.49	0.36	0.34	0.36	0.34
47 mm	0.40	0.45	0.42	0.45	0.49	0.61	0.51	0.61
87 mm	0.27	0.34	0.26	0.35	0.33	0.49	0.32	0.50
127 mm	0.38	0.35	0.37	0.38	0.45	0.42	0.43	0.45
167 mm	0.39	0.37	0.37	0.41	0.42	0.40	0.40	0.44
Internal	0.53	0.56	0.55	0.63	0.73	0.76	0.75	0.78

computation programs (Fortran code and COMSOL Multiphysics) have a large effect on the simulation results for the relative humidity, especially at the depth of 167 mm. The results of the two models have good consistency with the experimental results for Wall #4. Furthermore, the ME and RMSE of the relative humidity and temperature are within the

acceptable levels.

The above verification cases indicate that the simulation results of the two models agree well with the analytical solutions, the simulation results of the benchmark and the experimental data and that the difference in computation tools have little impact on the simulation results.

The difference between the simulation results of the two models is very small when the relative humidity is low. The errors in the relative humidity in the simulation results of the two models are both greater than those of the temperature. The deviations between the simulation and measurement results become greater when the relative humidity in the experimental conditions increases to the end of hygroscopic region.

4. Discussions

The above experimental validation uses two simulated methods (Fortran code and COMSOL Multiphysics) to demonstrate the accuracy of the Künzel model and the Liu model. There are still some deviations between the simulation and measurement values of each wall, and the deviations in relative humidity are greater than those in temperature. The sources of these deviations are discussed as follows.

(1) Errors from measurement method and sensors

The relative humidity sensors have lower measurement accuracy than the temperature sensors. This is one of the reasons that the ME and RMSE of the relative humidity are greater than those of temperature.

The temperature and humidity sensors are inserted into the measured walls by drilling, which might change the distribution of temperature and humidity and affect the measurement accuracy.

There are some missing and abnormal values in the measurements that are omitted in the simulation. This may lead to some large deviations between the simulation and measurement values due to the time discontinuity in the measurement.

(2) Deviations from material properties and input parameters

The test material in Section 3.3.3 was Scots pine. Pine and spruce were used to replace the Scots pine because of the unknown material properties of Scots pine, which might have resulted in the deviations between the simulation and measurement values in Fig. 4.

The material properties used in the simulation for Walls #1–#4 in Section 3.3.4 were from the Delphin material database [44], and the measured data were supplied by Rafidirason et al. [62] and Vololovirina et al. [63]. These properties might differ from the real material properties under experimental conditions. The materials in the experiments were anisotropic and their properties were dependent on the moisture content and temperature of materials in the experiments. However, the material property values used in the simulations were measured under constant temperature conditions and were only dependent on the moisture content of the materials.

The initial values at the measurement locations in Section 3.3.4 were very different at the beginning of the experiments. However, in the simulation, the initial values of the relative humidity at all locations were the same and taken as the measurement values of the middle locations at the beginning of the experiments. This may have resulted in some deviations during the beginning period of the simulation.

The surface heat and mass transfer coefficients were “fine-tuned” by running simulations with several values and choosing the values that generated the best results for the relative humidity and temperature at the external and internal surfaces of all walls, instead of being determined by the literature [56–58,62].

(3) Model deviations

The other significant reason for deviations in the simulated relative humidity is that both the dynamic models do not accurately depict the complex and nonlinear physical mechanism of coupled heat and moisture transfer process when porous building materials and envelopes are within the high relative humidity range. The two models use the relative humidity as the moisture driving potential. However, the moisture transport within porous building materials is combined with two flows:

vapor diffusion and liquid water transport. In low relative humidity (hygroscopic) regions, the moisture is mainly transported by vapor diffusion. It is reasonable that the relative humidity is used as the moisture driving potential of the models within low relative humidity regions. As the relative humidity increases, the amount of liquid water adhering to the pore walls in the material increases, and the liquid water transport increases under capillary action. When the relative humidity is close to or exceeds 95% (i.e., over-hygroscopic region), the moisture is primarily transported through liquid water which is mainly driven by capillary pressure. Both vapor and liquid transports can co-exist at the high end of the hygroscopic region [65]. Thus, as the relative humidity increases, the two models become more inaccurate, and the deviations between the simulation and measurement values become greater.

In addition, there are also some deviations between Fortran code and COMSOL Multiphysics simulation results. This may be due to: (1) differences in discretization methods—Fortran code uses the finite difference method, which is equally divided into N nodes; the commercial COMSOL Multiphysics software uses the finite element method and the mesh is more refined. (2) different material properties at the interface between two kinds of materials. Besides, in COMSOL Multiphysics simulations, a separate .mph file must be created to operate the simulation for each case, which cannot be integrated into a computing platform. But the Fortran code can be changed at any time according to users demands. Also, the simulation results of Fortran code can enhance the confidence of users to program and implement hygrothermal simulation calculations.

5. Conclusions

A considerable number of dynamic models for coupled heat and moisture transfer have been proposed in previous research. This study reviews and summarizes the model validation works in detail. Three categories of methods, theoretical validation, inter-model validation and experimental validation, were applied to validate the dynamic models of coupled heat and moisture transfer. A comprehensive validation was performed on two commonly used models, the Künzel model and the Liu model. The simulations were also carried out by two computation tools, self-programmed Fortran code and COMSOL Multiphysics for the two models. The verification showed that the simulation results of the two models agree well with the analytical solution, the simulation results of the benchmark and the experimental data and that the computation tools have little impact on the simulation results.

The two models have an acceptable accuracy in the hygroscopic range. Near over-hygroscopic region (relative humidity is less than but close to 95%), the Liu model is more accurate and applicable than the Künzel model. This indicated that they are both applicable for the hygrothermal performance simulation of porous building materials and envelopes in the hygroscopic range and the Künzel model is not applicable for hygrothermal simulations near over-hygroscopic region. Further validation is needed to validate whether the two models are applicable within the over-hygroscopic region when the relative humidity is greater than 95%. The impact of air infiltration or leakage on the hygrothermal performance of porous building materials and envelopes was not discussed in this study and it will be the focus of future work.

The heat and moisture transfer in building envelopes occur simultaneously and couple with each other, which significantly affects their hygrothermal performance, indoor air quality and environment, and structure durability. Therefore, this study boosts confidence for the application of the two popular dynamic models, Künzel model and Liu model, for coupled heat and moisture transfer in porous building materials and envelopes and provides a solid foundation for further post-processing simulation results of the two hygrothermal models to predict and evaluate the distributions of temperature and moisture content inside porous building materials and envelopes, to improve the hygrothermal performance of buildings, to predict the risk of mould growth

and to improve the durability of the structure. As for how to apply the simulation results of the two models in the post-processing work, further work by subsequent researchers is needed.

Author declaration

We wish to confirm that there are no known conflicts of interest associated with this publication and there has been no significant financial support for this work that could have influenced its outcome.

We confirm that the manuscript has been read and approved by all named authors and that there are no other persons who satisfied the criteria for authorship but are not listed. We further confirm that the order of authors listed in the manuscript has been approved by all of us.

We confirm that we have given due consideration to the protection of intellectual property associated with this work and that there are no impediments to publication, including the timing of publication, with respect to intellectual property. In so doing we confirm that we have followed the regulations of our institutions concerning intellectual property.

We understand that the Corresponding Author is the sole contact for

the Editorial process (including Editorial Manager and direct communications with the office). He/she is responsible for communicating with the other authors about progress, submissions of revisions and final approval of proofs. We confirm that we have provided a current, correct email address which is accessible by the Corresponding Author and which has been configured to accept email from ymchen@hnu.edu.cn.

CRediT authorship contribution statement

Wenqiang Dong: Software, Validation, Formal analysis, Investigation, Data curation, Writing - original draft, Visualization. **Youming Chen:** Conceptualization, Methodology, Writing - review & editing, Supervision, Project administration, Funding acquisition. **Yang Bao:** Software, Validation. **Aimin Fang:** Software, Resources.

Acknowledgments

This work was supported by “the 13th Five-Year” National Key R&D Program of China (Grant No. 2017YFC0702201).

Appendix A. Material properties and heat and mass transfer coefficients

Table A.1
Material properties of the wall in HAMSTAD Benchmark case #2 [28]

Material properties	Value/formula
Sorption isothermal (kg/m^3)	$w = \frac{116}{\left(1 - \frac{1}{0.118} \ln(\phi)\right)^{0.869}}$
Water vapor permeability (s)	$\delta_p = 1 \times 10^{-15}$
Moisture diffusivity (m^2/s)	$D_w = 6 \times 10^{-10}$
Liquid water permeability (s)	$K_l = \frac{(D_w \xi - \delta_p P_s) \phi}{R_D T p_l}$
Thermal conductivity ($\text{W}/(\text{m.K})$)	$\lambda = 0.15$
Specific heat capacity ($\text{J}/(\text{kg.K})$)	$c_{p,m} = 800$
Density (kg/m^3)	$\rho_m = 525$

Table A.2
Material properties of wall components in HAMSTAD Benchmark case #5 [28]

Material properties	Formula
Sorption isothermal w (kg/m^3)	$w = w_{\text{sat}} \cdot \sum_{i=1}^N \frac{b_i}{(1 + (-a_i \cdot R_D T \ln(\phi)/9.8)^{n_i})^{1-1/n_i}}$
Water vapor permeability δ_p (s)	$\delta_p = \frac{26.1 \cdot 10^{-6}}{\mu_{\text{dry}} R_D T} \frac{1 - w/w_{\text{sat}}}{(1 - p) \cdot (1 - w/w_{\text{sat}})^2 + p}$
Liquid water conductivity K_l (s)	$K_l(w) = \exp[\sum_{i=0}^5 k_i (w/\rho_w)^i]$

Table A.3
Parameters for all given materials in Table A2,[28]

Material property parameters	Brick	Mortar	Insulation
w_{sat} (kg/m^3)	373.5	700	871
b_1 (-)	0.46	0.2	0.41
b_2 (-)	0.54	0.8	0.59
a_1 ($1/\text{m}$)	0.47	0.5	0.006
a_2 ($1/\text{m}$)	0.2	0.004	0.012
n_1 (-)	1.5	1.5	2.5
n_2 (-)	3.8	3.8	2.4
μ_{dry} (-)	7.5	50	5.6
p (-)	0.20	0.20	0.20
k_0 (-)	-36.484	-40.425	-46.245
k_1 (-)	461.325	83.319	294.506
k_2 (-)	-5240	-175.961	-1439
k_3 (-)	2.907×10^4	123.863	3249
k_4 (-)	-7.41×10^4	0	-3370

(continued on next page)

Table A.3 (continued)

Material property parameters	Brick	Mortar	Insulation
k_5 (-)	6.997×10^4	0	1305
Thermal conductivity λ (W/(m.K))	0.682	$0.6 + 0.00056w$	$0.06 + 0.00056w$
Specific heat capacity $c_{p,m}$ (J/(kg.K))	1000	920	1000
Density ρ_m (kg/m ³)	1600	230	212

Table A.4

Material properties in the experiments of one-sided controlled conditions [27,58–61].

Material properties	Value/formula	Reference
Sorption isothermal (kg/m ³)	$w = \frac{168.54\phi}{(1 - 0.77\phi)(1 + 6.62\phi)}$	[59]
Water vapor permeability (s)	$\delta_p = 1.023 \times 10^{-14} \exp(\phi/0.1276) + 1.2216 \times 10^{-12}$	[60]
Moisture diffusivity (m ² /s)	$D_w = 1.4 \times 10^{-10}$	[58]
Liquid water permeability (s)	$K_l = \frac{(D_w \xi - \delta_p P_s)\phi}{R_D T \rho_l}$	[27]
Thermal conductivity (W/(m.K))	$\lambda = 0.11$	[61]
Specific heat capacity (J/(kg.K))	$c_{p,m} = 1880$	[61]
Density (kg/m ³)	$\rho_m = 400$	[61]

Table A.5

Material properties in the experiments of double-sided controlled conditions [44,62–64].

Wood fibreboard	Value	Refs
Thermal conductivity λ (W/(m.K))	$(0.28 \cdot H + (0.108 \cdot T + 38))/1000$	[63]
Water vapor resistance factor μ (-)	Dry cup: 6 Wet cup: 2	[63]
Dry bulk density ρ_m (kg/m ³)	150	[63]
Heat capacity $c_{p,m}$ (J/(kg.K))	$1600 + 4185 \cdot H$	[62]
Sorption isotherm w (kg/m ³)	Delphin material database	
Liquid water permeability K_l (s)		[44]
Water vapor permeability δ_p (s)		
External lime plaster	Value	Refs
Thermal conductivity λ (W/(m.K))	0.087	[64]
Water vapor resistance factor μ (-)	31	[62]
Dry bulk density ρ_m (kg/m ³)	1300	[62]
Heat capacity $c_{p,m}$ (J/(kg.K))	850	[62]
Sorption isotherm w (kg/m ³)	Delphin material database	
Liquid water permeability K_l (s)		[44]
Water vapor permeability δ_p (s)		
OSB	Value	Refs
Thermal conductivity λ (W/(m.K))	$((0.018 \cdot T - 0.072) \cdot \theta_m + (0.27 \cdot T + 89))/1000$	[63]
Water vapor resistance factor μ (-)	Dry cup: 46 Wet cup: 27	[63]
Dry bulk density (kg/m ³)	590	[63]
Heat capacity (J/(kg.K))	1700	[62]
Sorption isotherm w (kg/m ³)	Delphin material database	
Liquid water permeability K_l (s)		[44]
Water vapor permeability δ_p (s)		

Table A.6

Surface heat transfer and mass transfer coefficients in the simulation[64].

	1	2	3	4
h_e	20	16	19	19
h_i	10	7	6	4
β_e	5.8382×10^{-8}	5.8382×10^{-8}	5.8382×10^{-9}	5.8382×10^{-9}
β_i	1.8382×10^{-8}	5.8382×10^{-7}	5.8382×10^{-9}	5.8382×10^{-9}

Appendix B. Comparisons between experimental and simulation results under double-sided controlled conditions

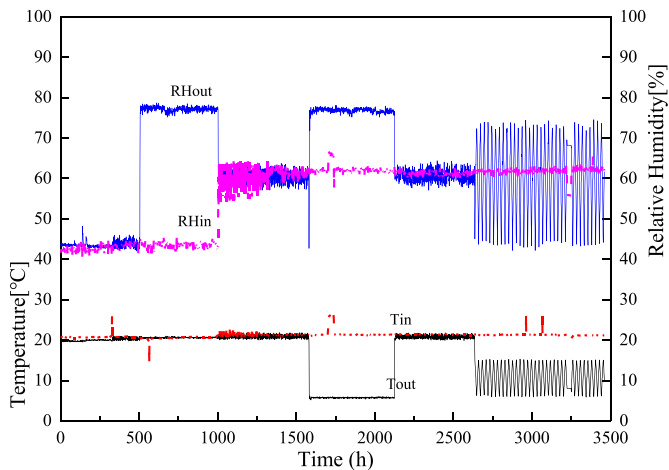


Fig. B.1. The relative humidity and temperature at the two sides of Wall #4 in the climate chamber (508–1008 h: isothermal conditions; 1584–2136 h: cooler conditions; 2640–3144 h: periodic climatic conditions).

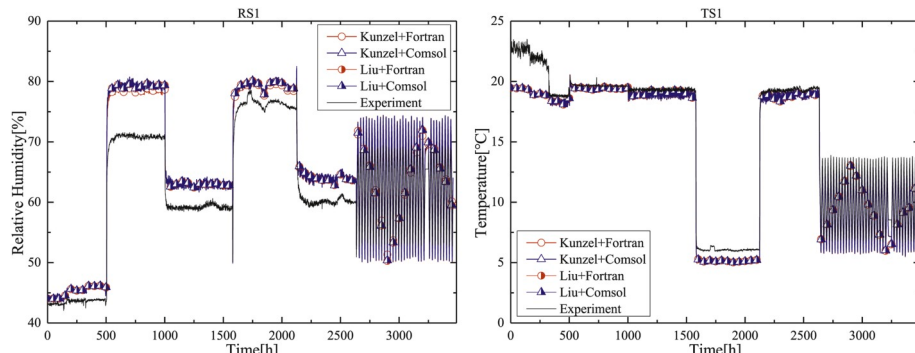


Fig. B.2. Comparison of relative humidity [%] (left) / temperature [°C] (right) at the external surface of Wall #1.

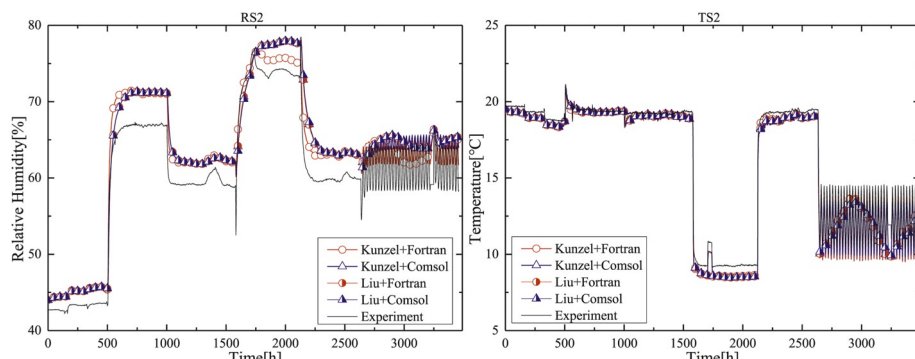


Fig. B.3. Comparison of relative humidity [%] (left) / temperature [°C] (right) at the depth of 20 mm in Wall #1.

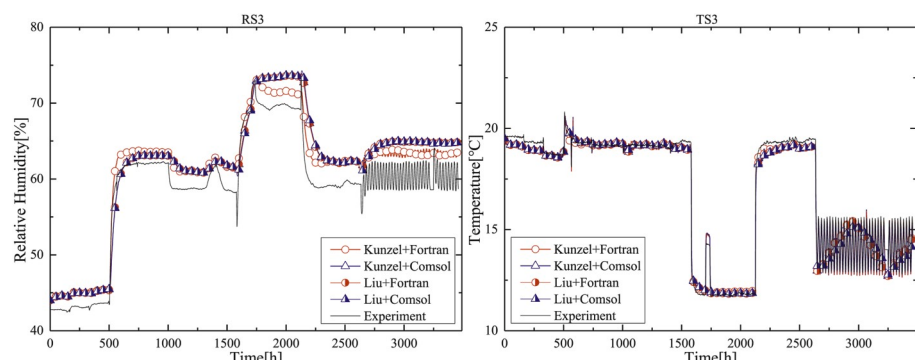


Fig. B.4. Comparison of relative humidity [%] (left) / temperature [°C] (right) at the depth of 40 mm in Wall #1.

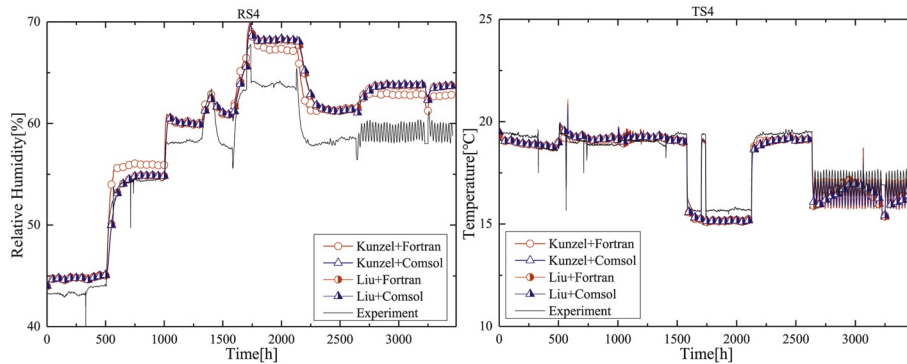


Fig. B.5. Comparison of relative humidity [%] (left) / temperature [°C] (right) at the depth of 60 mm in Wall #1.

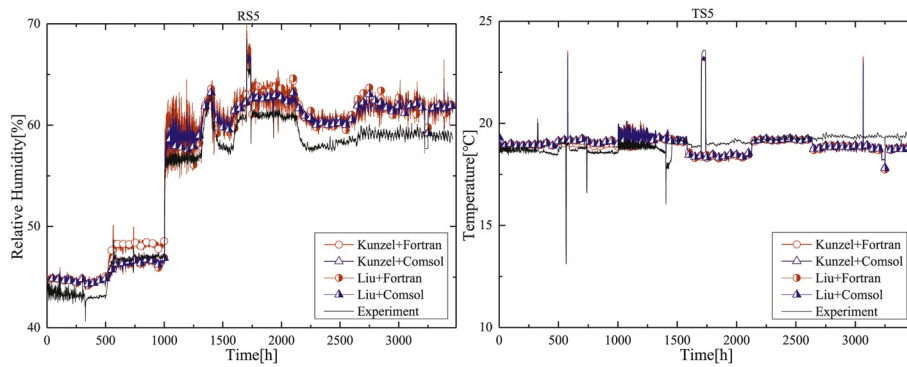


Fig. B.6. Comparison of relative humidity [%] (left) / temperature [°C] (right) at the internal surface of Wall #1.

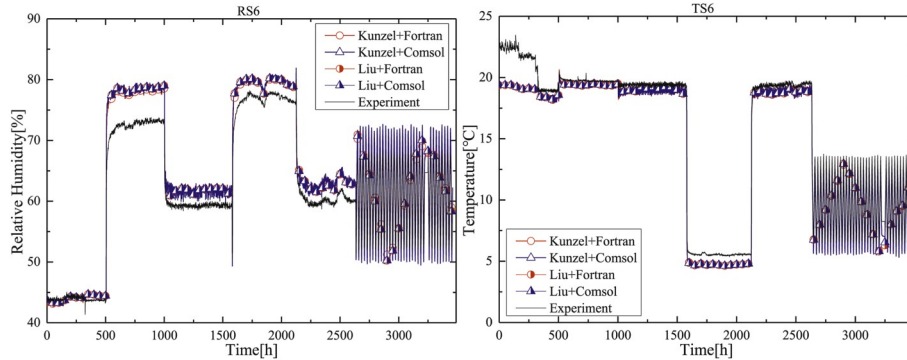


Fig. B.7. Comparison of relative humidity [%] (left) / temperature [°C] (right) at the external surface of Wall #2.

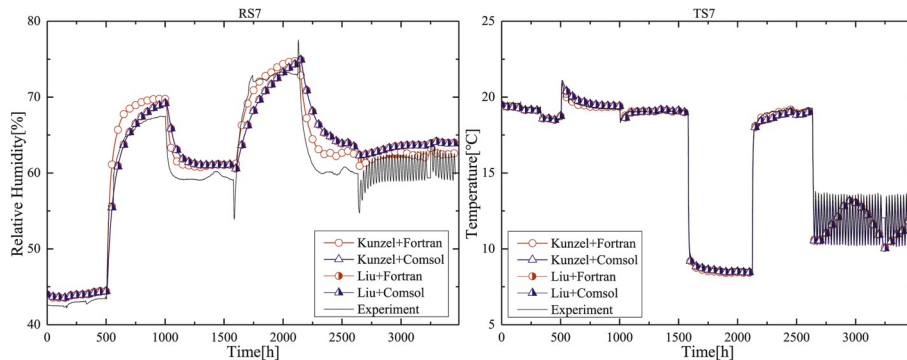


Fig. B.8. Comparison of relative humidity [%] (left) / temperature [°C] (right) at the depth of 40 mm in Wall #2.

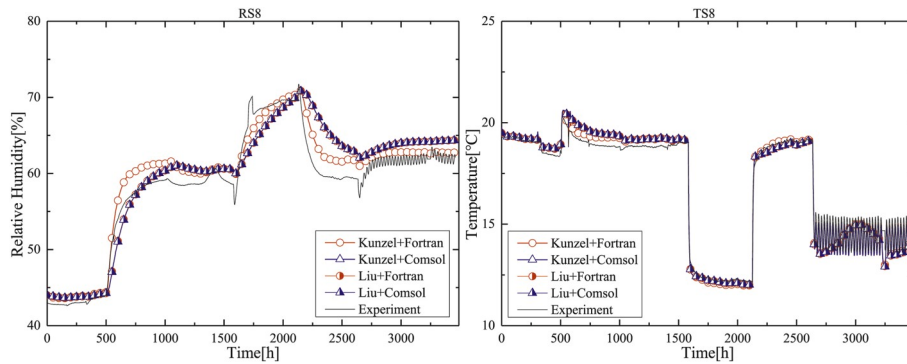


Fig. B.9. Comparison of relative humidity [%] (left) / temperature [°C] (right) at the depth of 80 mm in Wall #2.

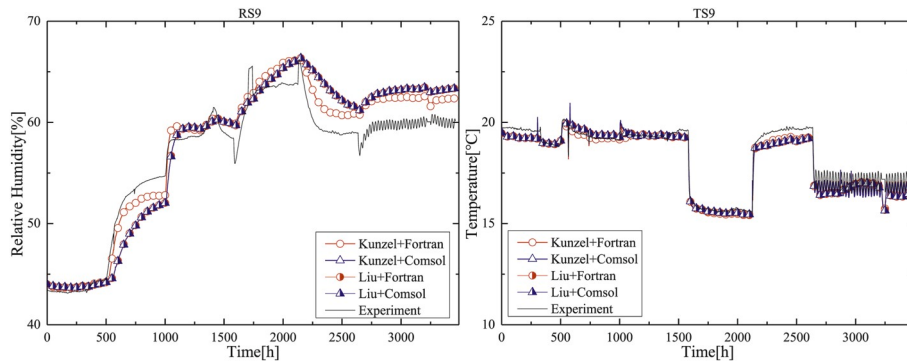


Fig. B.10. Comparison of relative humidity [%] (left) / temperature [°C] (right) at the depth of 120 mm in Wall #2.

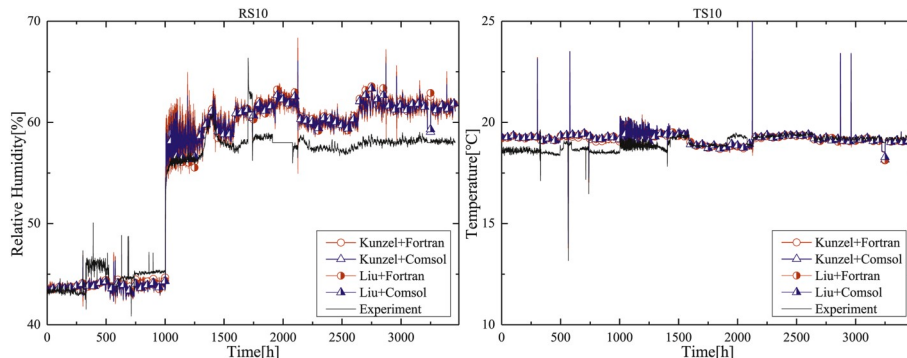


Fig. B.11. Comparison of relative humidity [%] (left) / temperature [°C] (right) at the internal surface of Wall #2.

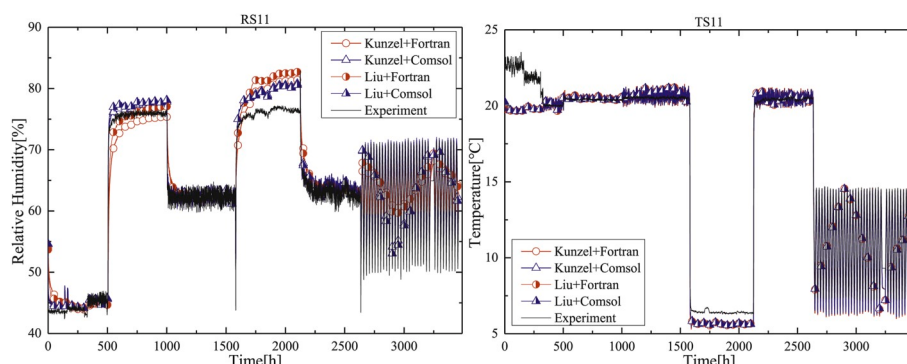


Fig. B.12. Comparison of relative humidity [%] (left) / temperature [°C] (right) at the external surface of Wall #3.

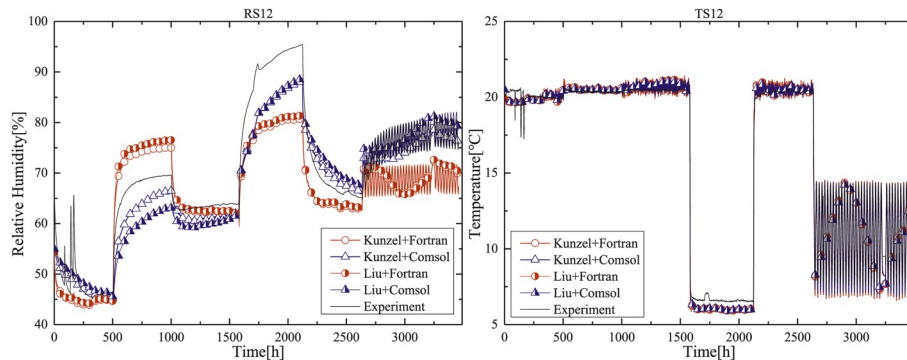


Fig. B.13. Comparison of relative humidity [%] (left) / temperature [°C] (right) at the depth of 7 mm in Wall #3.

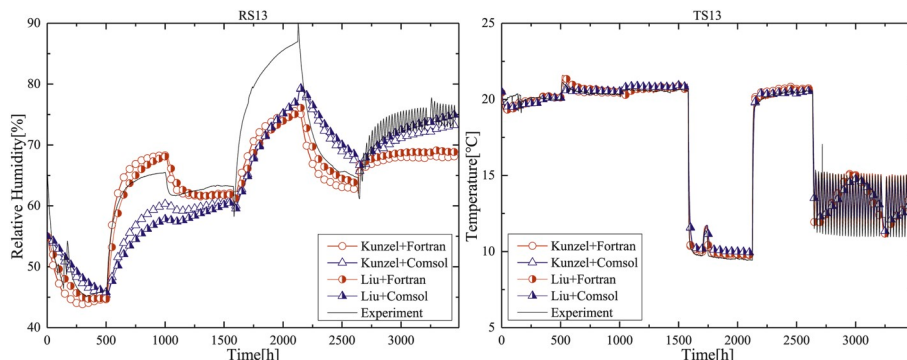


Fig. B.14. Comparison of relative humidity [%] (left) / temperature [°C] (right) at the depth of 47 mm in Wall #3.

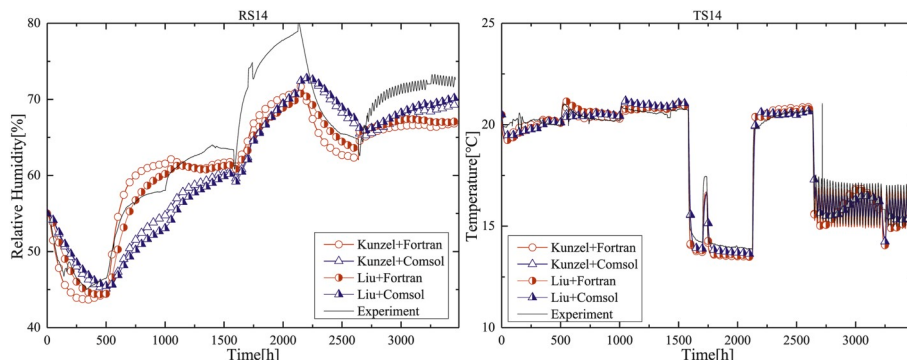


Fig. B.15. Comparison of relative humidity [%] (left) / temperature [°C] (right) at the depth of 87 mm in Wall #3.

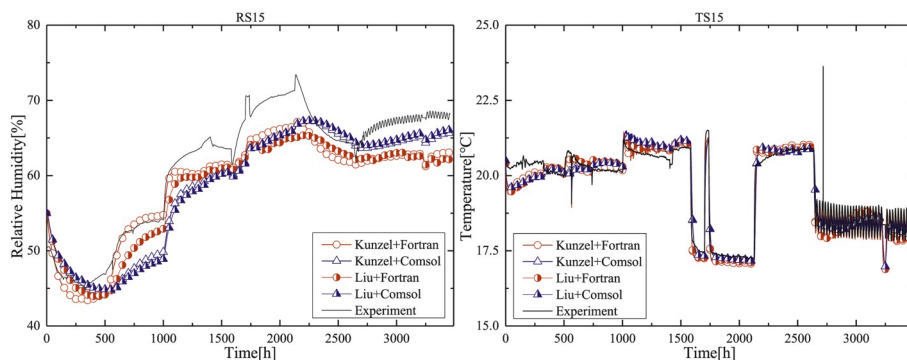


Fig. B.16. Comparison of relative humidity [%] (left) / temperature [°C] (right) at the depth of 127 mm in Wall #3.

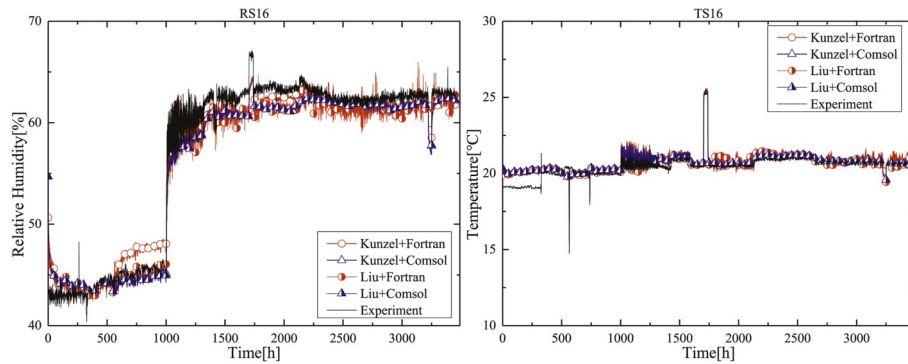


Fig. B.17. Comparison of relative humidity [%] (left) / temperature [°C] (right) at the internal surface of Wall #3.

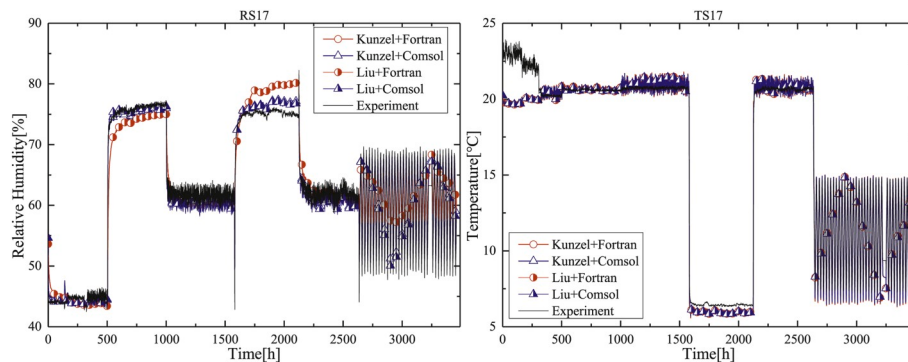


Fig. B.18. Comparison of relative humidity [%] (left) / temperature [°C] (right) at the external surface of Wall #4.

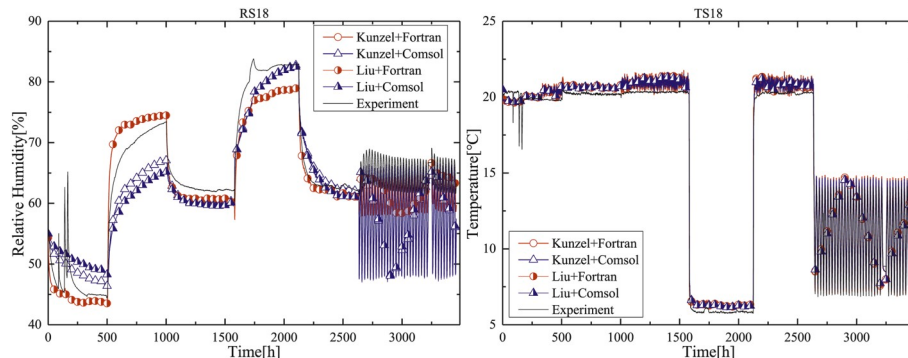


Fig. B.19. Comparison of relative humidity [%] (left) / temperature [°C] (right) at the depth of 7 mm in Wall #4.

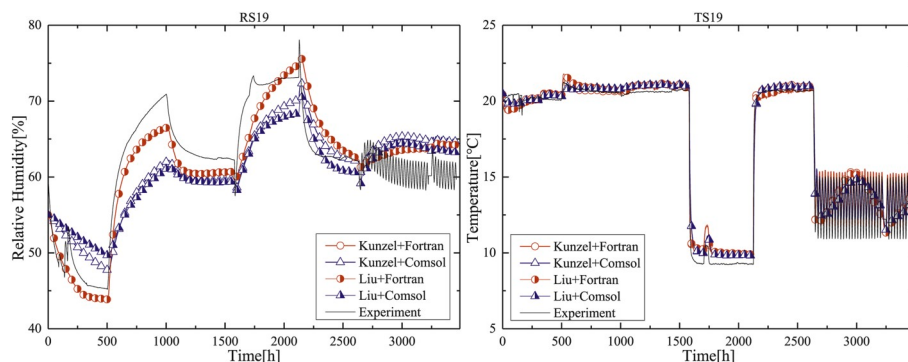


Fig. B.20. Comparison of relative humidity [%] (left) / temperature [°C] (right) at the depth of 47 mm in Wall #4.

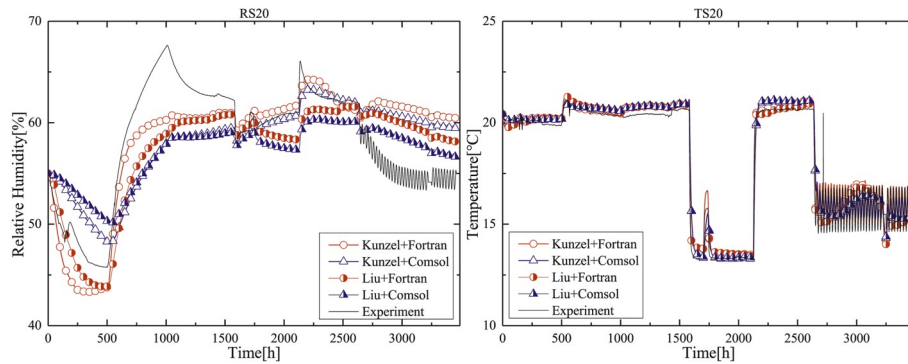


Fig. B.21. Comparison of relative humidity [%] (left) / temperature [°C] (right) at the depth of 87 mm in Wall #4.

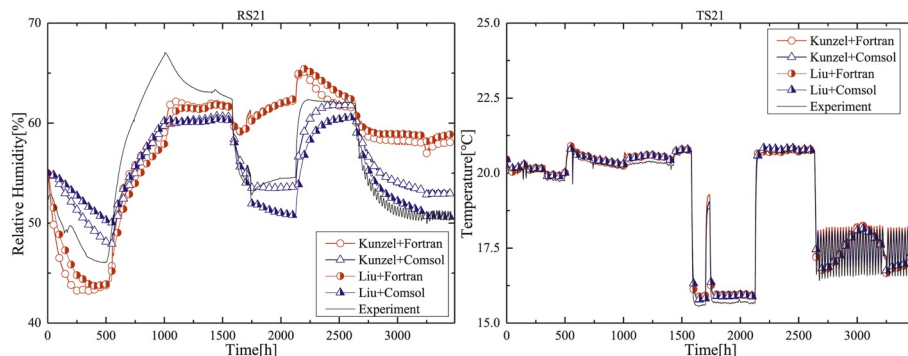


Fig. B.22. Comparison of relative humidity [%] (left) / temperature [°C] (right) at the depth of 127 mm in Wall #4.

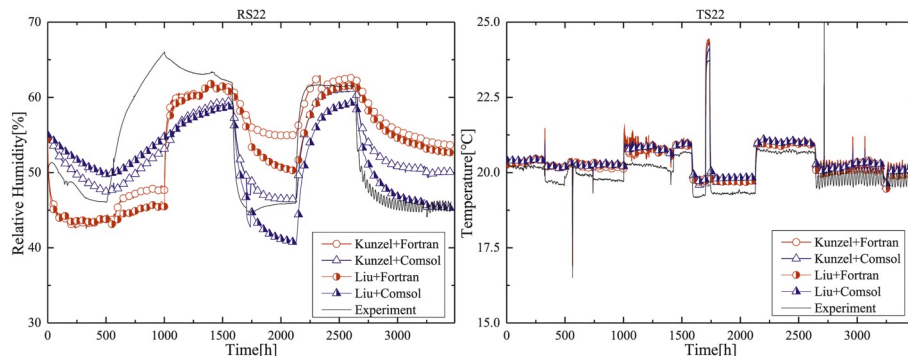


Fig. B.23. Comparison of relative humidity [%] (left) / temperature [°C] (right) at the depth of 167 mm in Wall #4.

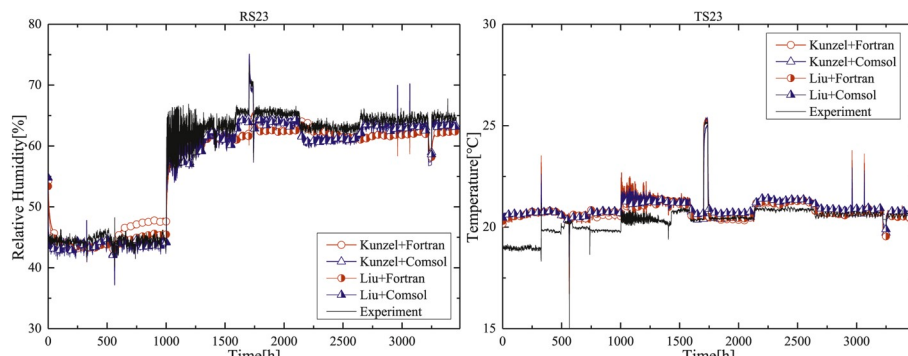


Fig. B.24. Comparison of relative humidity [%] (left) / temperature [°C] (right) at the internal surface of Wall #4.

References

- [1] N. Mendes, F.C. Winkelmann, R. Lamberts, P.C. Philippi, Moisture effects on conduction loads, *Energy Build.* 35 (7) (2003) 631–644.
- [2] R.M. Barbosa, N. Mendes, Combined simulation of central HVAC systems with a whole-building hygrothermal model, *Energy Build.* 40 (3) (2008) 276–288.
- [3] H.J. Moon, S.H. Ryu, J.T. Kim, The effect of moisture transportation on energy efficiency and IAQ in residential buildings, *Energy Build.* 75 (2014) 439–446.
- [4] F. Kong, M. Zheng, Effects of combined heat and mass transfer on heating load in building drying period, *Energy Build.* 40 (8) (2008) 1614–1622.
- [5] G.H. dos Santos, N. Mendes, Heat, air and moisture transfer through hollow porous blocks, *Int. J. Heat Mass Tran.* 52 (9–10) (2009) 2390–2398.
- [6] Y. Liu, Y. Wang, D. Wang, J. Liu, Effect of moisture transfer on internal surface temperature, *Energy Build.* 60 (2013) 83–91.
- [7] X. Liu, Investigation of the Coupled Heat, Air and Moisture Transport in Building Walls in Hot Summer and Cold Winter Zone, PhD Thesis, Hunan University, Hunan, 2015 (in Chinese).
- [8] A. Hukka, H.A. Viitanen, A mathematical model of mould growth on wooden material, *Wood Sci. Technol.* 33 (6) (1999) 475–485.
- [9] H. Viitanen, Factors Affecting the Development of Mould Growth and Brown Rot Decay in Wooden Materials and Wooden Structures, Effect of Humidity, Temperature and Exposure Time, PhD Thesis, The Swedish University of Agricultural Science, Department of Forest Products, Uppsala, 1996.
- [10] N.F. Jensen, S.P. Bjarlov, C. Rode, T.R. Odgaard, Hygrothermal assessment of internally insulated solid masonry walls fitted with exterior hydrophobization and deliberate thermal bridge, *ce/papers* 2 (4) (2018) 79–87.
- [11] P. Otv, Hygrothermal Modelling of Internal Insulation to Solid Masonry Walls (Master's Thesis), Kgs. Lyngby, Technical University of Denmark, Denmark, 2016.
- [12] P. Fazio, J. Rao, A. Alturkistani, H. Ge, Large scale experimental investigation of the relative drying capacity of building envelope panels of various configurations, Proceedings of the Third International Conference in Building Physics (IBPC3): Research in Building Physics and Building Engineering, Concordia University, Montreal, 2006, pp. 361–368.
- [13] A. Alturkistani, P. Fazio, J. Rao, Q. Mao, A new test method to determine the relative drying capacity of building envelope panels of various configurations, *Build. Environ.* 43 (12) (2008) 2203–2215.
- [14] H. Viitanen, J. Vinha, K. Salminen, T. Ojanen, R. Peuhkuri, L. Paajanen, K. Lähdesmäki, Moisture and bio-deterioration risk of building materials and structures, *J. Build. Phys.* 33 (3) (2009) 201–224.
- [15] M. Nofal, K. Kumaran, Biological damage function models for durability assessments of wood and wood-based products in building envelopes, *Eur. J. Wood Wood Prod.* 69 (4) (2011) 619–631.
- [16] H. Künzel, A. Karagiozis, A. Holm, A hygrothermal design tool for architects and engineers, in: Moisture Analysis and Condensation Control in Building Envelopes, ASTM Manual Series 50: Chapter 9, 2001.
- [17] A. Baughman, E. Arens, Indoor humidity and human health-Part I: literature review of health effects of humidity-influenced indoor pollutants, *Build. Eng.* 102 (1) (1996) 193–211.
- [18] M. Hosni, J. Sipes, Experimental results for diffusion and infiltration of moisture in concrete masonry walls exposed to hot and humid climates, *ASHRAE Transactions.* 105 (2) (1999) 191–203.
- [19] J.E. Christian, Moisture Sources, in: *Moisture Control in Buildings*, vol. 18, ASTM Manual Series: MNL, 1994, pp. 176–182.
- [20] J.R. Philip, D.A. De Vries, Moisture movement in porous materials under temperature gradients, *Eos, Transactions American Geophysical Union* 38 (2) (1957) 222–232, <https://doi.org/10.1029/TR038i002p00222>.
- [21] A.V. Luikov, Systems of differential equations of heat and mass transfer in capillary-porous bodies (review), *Int. J. Heat Mass Tran.* 18 (1) (1975) 1–14, [https://doi.org/10.1016/0017-9310\(75\)90002-2](https://doi.org/10.1016/0017-9310(75)90002-2).
- [22] D. Berger, D.C.T. Pei, Drying of hygroscopic capillary porous solids—a theoretical approach, *Int. J. Heat Mass Tran.* 16 (2) (1973) 293–302, [https://doi.org/10.1016/0017-9310\(73\)90058-6](https://doi.org/10.1016/0017-9310(73)90058-6).
- [23] P. Häupl, J. Grunewald, H. Fechner, H. Stopp, Coupled heat air and moisture transfer in building structures, *Int. J. Heat Mass Tran.* 40 (7) (1997) 1633–1642, [https://doi.org/10.1016/S0017-9310\(96\)00245-1](https://doi.org/10.1016/S0017-9310(96)00245-1).
- [24] Y. Goto, K.G. Wakili, T. Frank, T. Stahl, Y. Ostermeyer, N. Ando, H. Wallbaum, Heat and moisture balance simulation of a building with vapor-open envelope system for subtropical regions, *Build. Simul.* 5 (4) (2012) 301–314, <https://doi.org/10.1007/s12273-012-0086-3>.
- [25] N. Mendes, P.C. Philippi, A method for predicting heat and moisture transfer through multilayered walls based on temperature and moisture content gradients, *Int. J. Heat Mass Tran.* 48 (1) (2005) 37–51, <https://doi.org/10.1016/j.ijheatmasstransfer.2004.08.011>.
- [26] J.M.P.Q. Delgado, E. Barreira, N.M.M. Ramos, V.P. de Freitas, Hygrothermal simulation tools, in: J.M.P.Q. Delgado, E. Barreira, N.M.M. Ramos, V.P. de Freitas (Eds.), *Hygrothermal Numerical Simulation Tools Applied to Building Physics*, Springer Berlin Heidelberg, Berlin, Heidelberg, 2013, pp. 21–45, https://doi.org/10.1007/978-3-642-35003-0_3.
- [27] C.-E. Hagertoft, HAMSTAD WP2 Modeling, Version 4. Report-02:9, Department of Building Physics, Chalmers university of Technology, Gothenburg, 2002, pp. 1–3.
- [28] C.-E. Hagentoft, HAMSTAD-Final Report: Methodology of HAM-Modeling, Report R-02:8, Gothenburg, Department of Building Physics, Chalmers university of Technology, 2002, pp. 8–50.
- [29] F. Kong, H. Wang, Heat and mass coupled transfer combined with freezing process in building materials: modeling and experimental verification, *Energy Build.* 43 (10) (2011) 2850–2859, <https://doi.org/10.1016/j.enbuild.2011.07.004>.
- [30] C.R. Pedersen, *Combined Heat and Moisture Transfer in Building Constructions*, Technical University of Denmark, Thermal Insulation Laboratory, Denmark, September 1990. Report No. 214, doctoral thesis.
- [31] Q. Li, Development of a Hygrothermal Simulation Tool (HAM-BE) for Building Envelope Study, PhD Thesis, Concordia University, 2008.
- [32] COMSOL Multiphysics Website, 2019 accessed, <https://cn.comsol.com/>. (Accessed 15 July 2019).
- [33] H.M. Künzel, *Simultaneous Heat and Moisture Transport in Building Components*, Fraunhofer IRB Verlag, Stuttgart, 1995.
- [34] X. Liu, Y. Chen, H. Ge, P. Fazio, G. Chen, Numerical investigation for thermal performance of exterior walls of residential buildings with moisture transfer in hot summer and cold winter zone of China, *Energy Build.* 93 (2015) 259–268, <https://doi.org/10.1016/j.enbuild.2015.02.016>.
- [35] En, *Hygrothermal Performance of Building Components and Building Elements - Assessment of Moisture Transfer by Numerical Simulation*, 15206, British Standard, London, UK, 2007.
- [36] G. Chen, Q. Luo, X. Guo, X. Liu, M. Tu, Y. He, Study on mould germination risk in hygroscopic building wall, *Process Eng.* 205 (2017) 2712–2719, <https://doi.org/10.1016/j.proeng.2017.10.193>.
- [37] I. Budai, R. El-Diasty, A. Abdou, Modelling of moisture and thermal transient behaviour of multi-layer non-cavity walls, *Build. Environ.* 34 (5) (1999) 537–551, [https://doi.org/10.1016/S0360-1323\(98\)00041-9](https://doi.org/10.1016/S0360-1323(98)00041-9).
- [38] X. Guo, Research on Coupled Heat and Moisture Transfer Characteristics of Multilayer Walls in Hot and Humid Climate, PhD thesis, Hunan University, Hunan, 2010 (in Chinese).
- [39] M. Qin, R. Belarbi, A. Aït-Mokhtar, L.O. Nilsson, Coupled heat and moisture transfer in multilayer building materials, *Construct. Build. Mater.* 23 (2) (2009) 967–975, <https://doi.org/10.1016/j.conbuildmat.2008.05.015>.
- [40] M. Qin, A. Aït-Mokhtar, R. Belarbi, Two-dimensional hygrothermal transfer in porous building materials, *Appl. Therm. Eng.* 30 (16) (2010) 2555–2562, <https://doi.org/10.1016/j.applthermaleng.2010.07.006>.
- [41] S. Uttenbosch, *Risco Van Inwendige Condensatie in Een Externe Scheidingsconstructie*, Building Physics and Services, Eindhoven University of Technology, 2012.
- [42] H.M. Künzel, A. Karagiozis, 2 - hygrothermal behaviour and simulation in buildings, in: M.R. Hall (Ed.), *Materials for Energy Efficiency and Thermal Comfort in Buildings*, Woodhead Publishing, 2010, pp. 54–76, <https://doi.org/10.1533/9781845692771.54>.
- [43] I.B.P. Fraunhofer, Wufi, 2019 accessed, <https://wufi.de/de/>. (Accessed 15 July 2019).
- [44] BC Bauklimatek Dresden, Simulation Program for the Calculation of Coupled Heat, Moisture, Air, Pollutant, and Salt Transport, 2019 accessed, <http://bauklimatek-dresden.de/delphin/index.php?aLa=en>. (Accessed 15 July 2019).
- [45] A.W.M. van Schijndel, S. Goeten, H.L. Schellen, Simulating the complete HAMSTAD benchmark using a single model implemented in Comsol, *Energy Proc* 132 (2017) 429–434, <https://doi.org/10.1016/j.egypro.2017.09.651>.
- [46] O. López, I. Torres, A.S. Guimaraes, J.M.P.Q. Delgado, V.P. de Freitas, Inter-laboratory variability results of porous building materials hygrothermal properties, *Construct. Build. Mater.* 156 (2017) 412–423, <https://doi.org/10.1016/j.conbuildmat.2017.08.184>.
- [47] J.H. Park, Y. Kang, J. Lee, S.J. Chang, S. Wi, S. Kim, Development of wood-lime boards as building materials improving thermal and moisture performance based on hygrothermal behavior evaluation, *Construct. Build. Mater.* 204 (2019) 576–585, <https://doi.org/10.1016/j.conbuildmat.2019.01.139>.
- [48] Z. Huang, Y. Sun, F. Musso, Hygrothermal performance optimization on bamboo building envelope in Hot-Humid climate region, *Construct. Build. Mater.* 202 (2019) 223–245, <https://doi.org/10.1016/j.conbuildmat.2019.01.039>.
- [49] T.K. Hansen, S.P. Bjarlov, R.H. Peuhkuri, M. Harrestrup, Long term in situ measurements of hygrothermal conditions at critical points in four cases of internally insulated historic solid masonry walls, *Energy Build.* 172 (2018) 235–248, <https://doi.org/10.1016/j.enbuild.2018.05.001>.
- [50] M. Spierenburg, *Heat and Moisture in Wooden Bearings of Monumental Buildings*, (Graduation Report) Building Physics and Services, Eindhoven University of Technology, 28 Feb 2017.
- [51] T.Z. Desta, J. Langmans, S. Roels, Experimental data set for validation of heat, air and moisture transport models of building envelopes, *Build. Environ.* 46 (5) (2011) 1038–1046, <https://doi.org/10.1016/j.buildenv.2010.11.002>.
- [52] M. Van Belleghem, M. Steeman, A. Willockx, A. Janssens, M. De Paepe, Benchmark experiments for moisture transfer modelling in air and porous materials, *Build. Environ.* 46 (4) (2011) 884–898, <https://doi.org/10.1016/j.buildenv.2010.10.018>.
- [53] H.-J. Steeman, *Modelling Local Hygrothermal Interaction between Airflow and Porous Materials for Building Applications*, Ghent University, Faculty of Engineering, Ghent, Belgium, 2009.
- [54] T. Busser, J. Berger, A. Piot, M. Pailha, M. Woloszyn, Comparison of model numerical predictions of heat and moisture transfer in porous media with experimental observations at material and wall scales: an analysis of recent trends, *Dry. Technol.* (2018) 1–33, <https://doi.org/10.1080/07373937.2018.1502195>.
- [55] W. Tao, *Numerical Heat Transfer*, second ed., Xi'an Jiaotong University Press (Chinese Edition), 2001.
- [56] C. Bylund Melin, C.-E. Hagentoft, K. Holl, V.M. Nik, R. Kilian, Simulations of moisture gradients in wood subjected to changes in relative humidity and temperature due to climate change, *Geosciences* 8 (10) (2018) 378, <https://doi.org/10.3390/geosciences8100378>.
- [57] C. Bylund Melin, J. Bjurman, Moisture gradients in wood subjected to relative humidity and temperatures simulating indoor climate variations as found in

- museums and historic buildings, *J. Cult. Herit.* 25 (2017) 157–162, <https://doi.org/10.1016/j.culher.2016.12.006>.
- [58] C. Bylund Melin, T. Gebäck, A. Heintz, J. Bjurman, Monitoring dynamic moisture gradients in wood using inserted relative humidity and temperature sensors, *E-Preserv. Sci.* 13 (2016) 7–14.
- [59] L. Bratasz, A. Kozlowska, R. Kozlowski, Analysis of water adsorption by wood using the Guggenheim-Anderson-de Boer equation, *Eur J Wood Wood Prod* 70 (4) (2012) 445–451, <https://doi.org/10.1007/s00107-011-0571-x>.
- [60] C. Rode, C.O. Clorius, Modeling of moisture transport in wood with hysteresis and temperature dependent sorption characteristics, in: Performance of Exterior Envelopes of Whole Buildings IX, Oak Ridge National Laboratory, Oak Ridge, TN, USA, 2004, pp. 1–15.
- [61] M. Kumaran, IEA annex 24 final report, Task 3: Material properties. 3, IEA, Acco Leuven, 1996, pp. 14–132.
- [62] H. Rafidiarison, R. Rémond, E. Mougel, Dataset for validating 1-D heat and mass transfer models within building walls with hygroscopic materials, *Build. Environ.* 89 (2015) 356–368, <https://doi.org/10.1016/j.buildenv.2015.03.008>.
- [63] O. Vololonirina, M. Coutand, B. Perrin, Characterization of hygrothermal properties of wood-based products – impact of moisture content and temperature, *Construct. Build. Mater.* 63 (2014) 223–233, <https://doi.org/10.1016/j.conbuildmat.2014.04.014>.
- [64] A.J.P.M. Goeten, Hygrothermal Simulation Model: Damage as a Result of Insulating Historical Buildings. (Graduation Report) Building Physics and Services, Eindhoven University of Technology, Januari, 2016.
- [65] F. Tariku, K. Kumaran, P. Fazio, Transient model for coupled heat, air and moisture transfer through multilayered porous media, *Int. J. Heat Mass Tran.* 53 (15–16) (2010) 3035–3044, <https://doi.org/10.1016/j.ijheatmasstransfer.2010.03.024>.